Forward-backward asymmetry as a discovery tool for Z′ bosons at the LHC

Elena Accomando,[a] **Alexander Belyaev,**[a] **Juri Fiaschi,**[a] **Ken Mimasu,**[b] **Stefano Moretti**[a] **and Claire Shepherd-Themistocleous**[c]

[a]*School of Physics and Astronomy, University of Southampton, Highfield Campus,*
University Rd, Southampton, SO17 1BJ U.K.

[b]*School of Physics and Astronomy, University of Sussex,*
Falmer, Brighton, BN1 9RH U.K.

[c]*Particle Physics Department, STFC, Rutherford Appleton Laboratory,*
Harwell Science and Innovation Campus, Didcot, Oxfordshire, OX11 0QX U.K.

E-mail: E.Accomando@soton.ac.uk, A.Belyaev@soton.ac.uk,
Juri.Fiaschi@soton.ac.uk, K.Mimasu@sussex.ac.uk,
S.Moretti@soton.ac.uk, claire.shepherd@stfc.ac.uk

ABSTRACT: The Forward-Backward Asymmetry (AFB) in Z' physics is commonly only perceived as the observable which possibly allows one to interpret a Z' signal appearing in the Drell-Yan channel by distinguishing different models of such (heavy) spin-1 bosons. In this paper, we revisit this issue, showing that the absence of any di-lepton rapidity cut, which is commonly used in the literature, can enhance the potential of the observable at the LHC. We moreover examine the ability of AFB in setting bounds on or even discovering a Z' at the Large Hadron Collider (LHC) concluding that it may be a powerful tool for this purpose. We analyse two different scenarios: Z'-bosons with a narrow and wide width, respectively. We find that, in the first case, the significance of the AFB search can be comparable with that of the 'bump' search usually adopted by the experimental collaborations; however, in being a ratio of (differential) cross sections, the AFB has the advantage of reducing experimental systematics as well as theoretical errors due to PDF uncertainties. In the second case, the AFB search can outperform the bump search in terms of differential shape, meaning the AFB distribution may be better suited for new broad resonances than the event counting strategy usually adopted in such cases.

Contents

1 Introduction

Heavy neutral Z'-bosons arise in a number of theories that extend the Standard Model (SM) gauge group by adding an extra U(1) symmetry. The most common Z'-boson benchmark models can be divided in three main classes: E_6 models, Generalized Left-Right (GLR) symmetric models and Generalized Standard Models (GSM), see, e.g., the reviews in [1, 2] and references therein. All of these models predict a relatively narrow width for the Z'-bosons, with $\Gamma_{Z'}/M_{Z'}$ lying in the 0.5–12% range. The lowest $\Gamma_{Z'}/M_{Z'}$ value is realised in the E_ψ model from the E_6 class while the biggest value appears in the Q-model belonging to the GSM class.

Experimental searches for a heavy Z'-boson at the LHC are usually interpreted in the context of the Sequential Standard Model (SSM), which is part of the GSM class [3]. This benchmark scenario just includes one extra neutral vector boson with couplings to fermions identical to those of the corresponding SM Z-boson and no mixing with the neutral Electro-Weak (EW) SM bosons. Being nothing but a heavier copy of the SM Z-boson, this Z'-boson is characterized by a narrow width: $\Gamma_{Z'}/M_{Z'} \simeq 2.8\%$, including the Z'-decay into top-antitop pairs above threshold. Dedicated search strategies therefore assume that the new heavy resonance is narrow and can be described by a Breit-Wigner line-shape, standing over the SM background, when looking at the invariant mass distribution of the Z'-boson decay products. In this way, the new physics signal is thought to have a well defined peaking structure, concentrated in a small interval centred around its mass. On the basis

of this assumption, the 95% Confidence Level (C.L.) upper bound on the cross section is derived and limits on the mass of the Z'-boson are extracted within the above mentioned benchmark models. In the case of a narrow width Z' scenario, even interference effects can be accounted for without substantially altering the described experimental approach [4, 5].

However, the narrow width hypothesis is quite strong, even if well motivated. There exist counter examples of theories where the predicted Z'-boson is characterized by a large width. For example, this can be realized in Technicolor [6] scenarios, Composite Higgs Models [7] or in more generic setups where the Z'-boson couples differently to the first two fermion generations with respect to the third one [8, 9] or else interacts with the SM gauge bosons in presence of mixing [10], so that large $\Gamma_{Z'}/M_{Z'}$ values are induced by the additional Z' decay channels present in such cases. As a consequence, the resulting wide resonance, instead of having a well defined Breit-Wigner line shape, will appear as a broad shoulder spreading over the SM background. In such models the ratio $\Gamma_{Z'}/M_{Z'}$ can easily reach 50% or higher, making a Breit-Wigner line shape based analysis inappropriate.

First phenomenological studies have been performed using a Bayesian statistical method and exclusion bounds on the Z'-boson mass have been estimated [11]. However, the experimental collaborations have not yet tackled this kind of scenario and dedicated search strategies for wide Z' particles are absent at the moment. The only frameworks which have been analyzed in order to interpret possible non-resonant deviations from the SM are the graviton production within the ADD model [12, 13] and the contact interaction within the left-left isoscalar model [14, 15]. For details on the parametrization of the differential cross section within these two scenarios we refer to ref. [16] and references therein. Both processes might give rise to an excess of events spread over the SM background. In this 'effectively' non-resonant case, the experimental analyses are essentially counting experiments: an excess of events sought out of an estimated SM background. To make the analyses more robust, the same background is often estimated with multiple data-driven methods. Kinematical cuts are then optimized in order to maximize the discovery/exclusion potential at the LHC. Despite this, as one can understand, this analysis can be fragile. The experimental results heavily rely on a good understanding and control of the SM background, as the new physics signal is not expected to have a definite shape. The choice of the control region, needed to define the functional form of the SM background to be used in the regions where there might be some signal, is not trivial. Interference effects between a new physics signal and the SM background can indeed affect the low scale region of the distribution in the invariant mass of the Z'-boson decay products, proving the assumption that the control region is new physics free to be simply false. Under these premises the experimental analyses could get quite complicated. On the one hand, the possible presence of wide objects could in fact deplete the 'new physics free' region, owing to an increase of the interference effects driven by the large width. On the other hand, the wide Z'-bosons could easily escape detection in the bump searches due to the same interference effects combined with the absence of a resonant peaking structure in, e.g., the di-lepton invariant mass distribution. All of this can conspire to make the discovery of a wide Z' very problematic. The importance of such effects has been highlighted in refs. [4, 5, 17]. The same level of complication arises when searching for heavy charged W'-bosons as described in

refs. [5, 17, 18]. For that search, which also relies on a counting strategy as no Breit-Wigner can appear owing to the presence of the neutrino in the leptonic Drell-Yan channel, the CMS collaboration recently included the interference effects between the extra W' and the SM W-boson [19, 20].

In this paper, we focus on the Z'-boson search and study the potential of a second observable, complementary to the di-lepton invariant mass used by default, in order to maximize the sensitivity to new massive Z' objects, either narrow or broad. The variable we analyse is the Forward-Backward Asymmetry (AFB). In the literature, this observable is usually advocated in the second stage of the data analysis process to interpret experimental results after a possible discovery of a new spin-1 particle using a standard bump hunt. The AFB can be used to disentangle different models with Z'-bosons and nail down the underlying theory. This procedure relies on the assumption that the new heavy Z'-boson is characterized by a narrow width and it would be discovered via the bump search. Our purpose is to show that the AFB can be used not only for interpreting a possible discovery but also in the very same search process. We show that the AFB observable can be associated to the default resonance search to improve and/or extend the discovery potential for both narrow and wide Z's. Focussing on AFB, we aim at establishing the methods needed to study Z'-boson production at the CERN LHC in the Drell-Yan channel, giving rise to di-lepton pairs in the final state: $pp \to l^+ l^-$ with $l = e, \mu$. This production process is particularly clean and thus represents the golden channel for Z'-boson discovery at the LHC.

The paper is organized as follows. In section 2, we derive current and projected bounds for Z' model benchmarks for the LHC at 8 and 13 TeV, respectively, for the models presented in ref. [1]. In section 3, we discuss the role of the forward-backward asymmetry within the Z' physics, its reconstruction and statistical uncertainty. We also discuss the effect of a rapidity cut on the di-lepton system upon the signal significance. This cut is commonly implemented in order to increase the efficiency in guessing the quark direction in pp collisions, which is needed to reconstruct the AFB observable. The drawback of applying it is a decrease of the number of signal events with the consequent depletion of the AFB significance. The outcome is that this stringent cut can be relaxed for the range of Z'-boson masses which we will be looking for in the next LHC run. In section 4, we discuss the role of the AFB in searches for narrow width Z'-bosons and systematically analyse Z' model benchmarks confronted with AFB and bump searches. We will show that the significance from the AFB can be comparable with that obtained from the cross section studies over the same invariant mass distribution of the di-lepton system. In this scenario, the advantage of using the AFB observable would consist in minimizing the systematics, as the AFB is a ratio of (differential) cross sections. Moreover, the two observables (cross section and asymmetry) could be of mutual support to make the claim of a possible new physics discovery more robust, if the bump search itself would provide only mild evidence for a Z' state.

In section 5, we analyse the role of AFB in searches for wide Z' particles. We consider two benchmark models which predict a wide Z'-boson with ratio $\Gamma_{Z'}/M_{Z'}$ of the order of several tens of percent. In this case, again, the AFB can be complementary to the resonance

search and have a distinctive line shape contrary to the invariant mass distribution of the cross section, which could well mimic the background shape. That is, the latter would only give rise to an excess of events evenly spread over the SM background, which is of difficult interpretation and in many cases of difficult measurement owing to uncertainties in the background modelling. In section 6, we discuss the Parton Distribution Function (PDF) uncertainties at the energy scale where we expect to find new Z'-bosons at the LHC. Our finding is that, even if the design luminosity $\mathcal{L} = 300\,fb^{-1}$ is reached at the LHC Run II, the AFB can play an important role in the narrow (and wide) Z'-boson hunt. The reason is that, even if a striking new physics signal with low statistical error were to be found in the bump search, its theoretical interpretation could be very poor owing to the severe PDF uncertainty affecting the di-lepton invariant mass distribution. The PDF error can be indeed much bigger than the statistical one and the gap grows with incresing luminosity. In this case, the AFB measurement could be of valuable help. We show in fact that the AFB error is dominated by statistics, as the PDF uncertainties largely cancel in the ratio between cross sections, so it can only improve with the luminosity. Finally, in section 7 we summarize and conclude.

2 Bounds on the Z'-boson mass

In this section, we re-derive the existing bounds on the mass of the Z'-boson from the aforementioned benchmarks models as obtained by, e.g., the CMS collaboration, after the 7, 8 TeV run with about 20 fb^{-1} of accumulated luminosity, assuming a narrow width. These can be found in ref. [16]. After confirming current CMS limits obtained under the above assumption, we further present those obtained by taking into account the full width effect as well the intereference corrections. Finally, we produce projected limits for LHC Run 2.

We therefore start by scanning over the thirteen benchmark models predicting a Z'-boson characterized by a narrow width ($\Gamma_{Z'}/M_{Z'} \leq 5\%$) summarized in ref. [1], and extract the limits on $M_{Z'}$ by making use of the 95% C.L. upper bound on the Z'-boson production cross section in Drell-Yan, $\sigma(pp \to Z' \to e^+e^-, \mu^+\mu^-)$. In order to reduce systematic uncertainties, the experimental analysis normalizes the Z'-boson production cross section in Drell-Yan to the SM Z-boson cross section on peak. As shown in figure 1, the 95% C.L. upper bound is indeed given on the ratio $R_\sigma = \sigma(pp \to Z' \to e^+e^-, \mu^+\mu^-)/\sigma(pp \to Z, \gamma \to e^+e^-, \mu^+\mu^-)$. The use of this ratio R_σ in fact cancels the uncertainty in the integrated luminosity and reduces the dependence on the experimental acceptance and trigger efficiency.

We calculate this ratio, R_σ, at the Next-to-Next-to-Leading Order (NNLO) in QCD using the WZPROD program [21–23] (which we have adapted for Z' models and new PDF sets [1]) and the CTEQ6.6 package [24]. Similar computations have been performed in ref. [17], albeit within a different kinematical setup. There, the R_σ ratio is evaluated at NLO+NLL using RESUMMINO. The NNLO QCD contributions give rise to a K-factor which depends on the energy scale, thus we fully take into account such a dependence. The NNLO prediction for the SM Z, γ production cross section, $\sigma(pp \to Z, \gamma \to l^+l^-)$ with
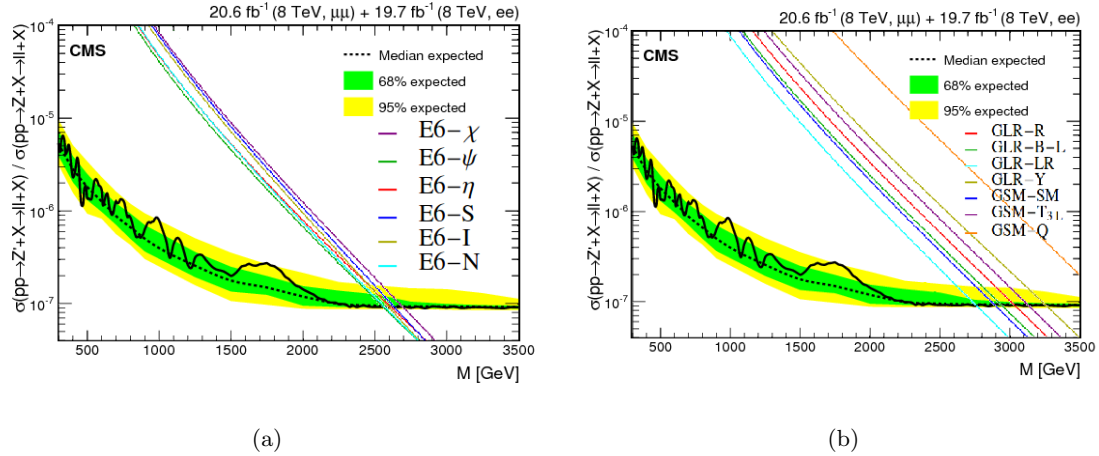
Figure 1. (a) 95% C.L. upper bound on the Z'-boson production cross section in Drell-Yan normalized to the SM cross section on the Z-boson peak: $R_\sigma = \sigma(pp \to Z' \to l^+l^-)/\sigma(pp \to Z, \gamma \to l^+l^-)$ with $l = e, \mu$. The combined analysis of the di-muon and di-electron channels has been produced by the CMS collaboration with a data sample collected at the 8 TeV LHC, corresponding to an integrated luminosity of 20.6 and 19.7 fb^{-1} respectively [16]. Theoretical predictions for the class of the E_6 models are superimposed to extract the corresponding Z'-boson mass limits. As described in the text, in order to match theoretical predictions and experimental results, the optimal cut on the invariant mass of the di-lepton pairs has been implemented: $\Delta M = |M_{ll} - M_{Z'}| \leq 0.05 \ E_{\mathrm{LHC}}$ for $E_{\mathrm{LHC}} = 8 \, \mathrm{TeV}$. (b) Same as (a) for the other two classes of GSM and GLR models.

$l = e, \mu$, in the mass window of 60 to 120 GeV is 1.117 nb. With all these ingredients at hand, we compute R_σ as a function of the mass of the new heavy Z'-boson, $M_{Z'}$, and derive the corresponding limits for all benchmark models. Figure 1(a) shows the bounds on all E_6 models, while figure 1(b) displays the results for the remaining two classes of models, GLR and GSM. As previously mentioned, traditional experimental analyses work under the hypothesis that the signal has a Breit-Wigner line shape and performs the analysis in a restricted search window around the hypothetical mass of the Z'-boson. This approach is theoretically motivated by the benchmark models, all predicting a narrow width Z'-boson, and by the will to perform as model independent an analysis as possible. One should stress that the CMS analysis makes use of a dedicated cut on the invariant mass of the di-lepton pairs: $|M_{l\bar{l}} - M_{Z'}| \leq 0.05 \times E_{\mathrm{LHC}}$ where E_{LHC} is the collider energy. This cut was designed so that the error in neglecting the (model-dependent) Finite Width (FW) and interference effects (between γ, Z, Z') is kept below $O(10\%)$ for all models and for the full range of allowed Z' masses under study, following the recommendations of [4, 5].

This procedure thus continues to allow for a straightforward interpretation of the extracted mass bounds in the context of any theory predicting a narrow Z'-boson. At this stage of our own analysis, we work under the very same setup, for validation purposes, with the notable exception that we allow for the aforementioned FW and interference effects, unlike the experimental results which assume the so-called Narrow Width Approximation (NWA), wherein the (narrow) Z' is actually produced on-shell. Table 1 summarizes the bounds we obtain. They reproduce the CMS limits very well in general, within the accuracy

Class	E_6						GLR				GSM		
$U'(1)$ Models	χ	ψ	η	S	I	N	R	$B-L$	LR	Y	SM	T_{3L}	Q
$M_{Z'}$ [GeV]	2700	2560	2620	2640	2600	2570	3040	2950	2765	3260	2900	3135	3720

Table 1. Bounds on the Z'-boson mass derived from the latest direct searches performed by CMS at the 8 TeV LHC with integrated luminosited $\mathcal{L} = 20\,fb^{-1}$. We consider thirteen different models with an extra $U'(1)$ gauge group predicting a new heavy neutral boson characterized by a narrow width. From left to right, the columns indicate the $M_{Z'}$ limit in GeV within the E_6, GLR and GSM class of models.

of 1–2%. The only slight exception is the Q-model in the GSM class where our limit, based on the present analysis accounting for full width and interference, is different from the CMS one by about 5%. This is well in line with expectations, as this model is the one yielding the largest width. But let us set the stage in some more detail. In figure 2 we show the behaviour of the new physics signal for two representative scenarios: the E_ψ model (figure 2(a)) and the SSM benchmark scenario (figure 2(b)). The solid line represents the full new physics signal, that is, Z'-boson production and decay including the interference with the SM background. The dashed line gives instead the pure Z'-boson signal, neglecting the interference. (As evident from the plots, in both cases we allow for FW effects of the Z'-boson.) As one can see, the shape of the distribution in the invariant mass of the di-lepton system is quite model dependent off peak due to the presence of large interference effects. The sign of the interference is not defined a priori. It can be either positive, like in the majority of the E_6 models, or negative, like in the two other classes of GLR and GSM models. In addition, its magnitude can be quite sizeable. For a detailed description of the behaviour of the interference between the new Z'-boson and the SM background we refer to refs. [4, 11], where the models with maximal constructive and destructive interference have been identified.

The off peak tail of the signal distribution in the di-lepton invariant mass is thus highly model dependent in the low mass region, leading to either an excess or a depletion of the total number of expected events as compared to the SM background, according to the sign of the interference.

Furthermore, it is clear that the fully integrated cross section for the complete new physics signal, that is, Z'-boson production and decay including the interference with the SM background, is not always a uniquely defined variable. In the SSM, and more generally in all GSM and GLR models, the signal can manifest itself as a negative correction to the differential cross section (solid line) at low masses. Similarly, the fully integrated cross section for the pure Z'-boson production and decay, neglecting the interefences, can also give an incorrect picture. Taking into account the low mass tail of the invariant mass distribution can overestimate the Z'-boson signal by a large factor. For a SSM Z' with mass $M_{Z'} = 3\,\text{TeV}$, we have that the fully integrated cross section for the pure signal is $\sigma_{Z'} = 0.17\,fb$ while the complete signal cross section, integrated in the mass window where it is positive definite, is equal to $\sigma_{Z'} + \text{Interference} = 0.06\,fb$. In this case, taking into account the unphysical tail (which in the SSM is in reality washed out by the destructive interference) leads to an overestimate the Z' signal by a factor of 3 and consequently the
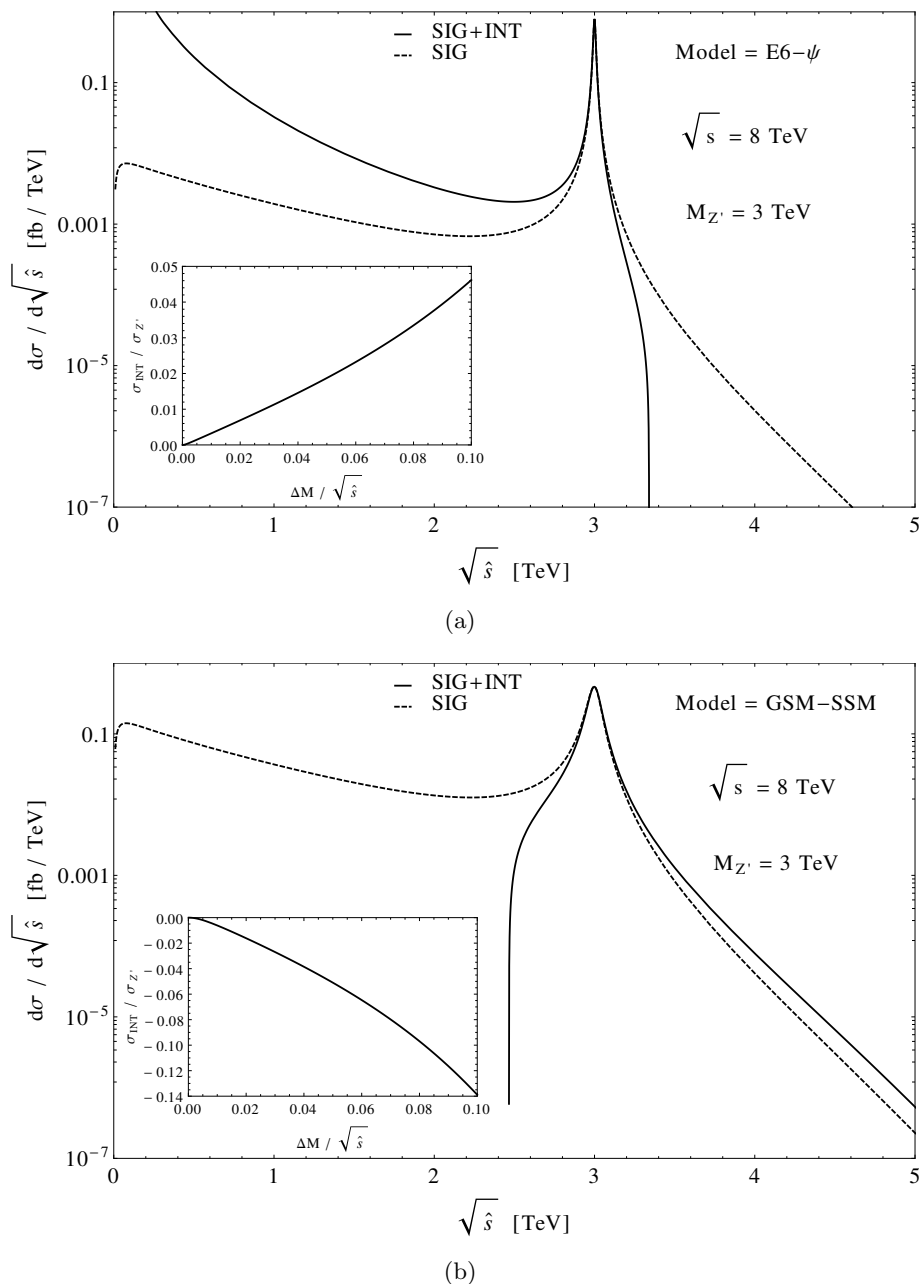
Figure 2. (a) Differential cross section in the invariant mass of the di-lepton system coming from the Z'-boson production and decay in the Drell-Yan channel: $pp \rightarrow e^+e^-$. We consider the E_ψ model. The solid line shows the complete new physics contribution to the invariant mass distribution, that is the Z' signal plus the interference with the SM background. The dashed line represents instead the pure Z' signal, neglecting the intereference. The inset plot displays the ratio between the interference contribution and the pure Z' signal. All curves have been produced for the 8 TeV LHC. No cuts are applied. (b) Same for the SSM benchmark scenario.

extraction of more stringent, erroneous limits. In essence, a shape analysis of the signal over the full invariant mass region is very challenging. Thus, the definition of the observable to be used to interpret the data and extract the mass bounds on the hypothetical Z'-boson must indeed be appropriately chosen.

However, thanks to the approach recommended in [4, 5], all such extreme effects are avoided and, in the instance, we can conclude that our code for the simulation of Drell-Yan processes which might receive a contribution from a narrow Z'-boson exchange, $pp \to \gamma, Z, Z' \to l^+l^- (l = e, \mu)$, has been validated against the CMS results. In short, by finally taking into account the published acceptance $\times$ efficiency corrections $(A \times \epsilon)$, we can indeed reproduce the above mentioned extracted bounds on the Z'-boson mass by self-consistently evaluating signal and background. In doing so, we have applied Poisson statistics for computing the significance, defining a 5σ observation as a discovery and excluding new physics up to 2σ when deriving limits on $M_{Z'}$. Here, 5σ (2σ) observation means a new physics effect at the level of 5(2) standard deviations away from the expected number of events within the SM.

With these definitions and using the abovementioned code, in figures 3 and 4, we now project discovery and exclusion potential of the upgraded LHC, which will run at $13\,\mathrm{TeV}$. The first two plots show the LHC discovery potential for the E_6 models (figure 3(a)) and for the remaining two classes GLR and GSM (figure 3(b)). The discovery reach that we find is in accordance with the results published in the Snowmass white paper [25] and references therein. Figures 4(a) and 4(b) display instead the LHC exclusion potential for E_6, GSM and GLR models, respectively. In deriving these results, we stress that we have included the $A \times \epsilon$ factor extracted by the analyses performed by CMS at the $8\,\mathrm{TeV}$ LHC, thereby implicitly assuming that no significant departures in this respect occur at the upgraded CERN machine. These projections are valid only for narrow width Z'-bosons for which the optimal observable is the invariant mass of the di-lepton system, used in the standard bump search performed by the experimental collaborations. From the above plots, one can conclude that the $13\,\mathrm{TeV}$ run of the LHC should be able to discover a Z'-boson with mass up to about $4500\,\mathrm{GeV}$ and $5600\,\mathrm{GeV}$ within the E_6 and GSM/GLR class of models, respectively. If nothing is found, the exclusion limits will be pushed up to $5300\,\mathrm{GeV}$ and $6400\,\mathrm{GeV}$ for an E_6 Z'-boson and a GSM/GLR Z'-boson, respectively. Table 2 summarizes the LHC Run II potential for a Z'-boson of a certain mass within all considered thirteen models. These projections have been obtained for the design value of the integrated luminosity: $\mathcal{L} = 300\,fb^{-1}$.

This concludes the section on the state-of-the-art of narrow width Z'-bosons and their search using traditional methods.

3 The forward-backward asymmetry

In this section, we define the forward-backward charge asymmetry (AFB) and discuss its role in Z'-boson searches other than the interpretation of an observed resonance. In the literature, the AFB has been long exploited to help disentangle the various theories predicting an extra heavy neutral boson and tracing back the Lagrangian parameters (see,
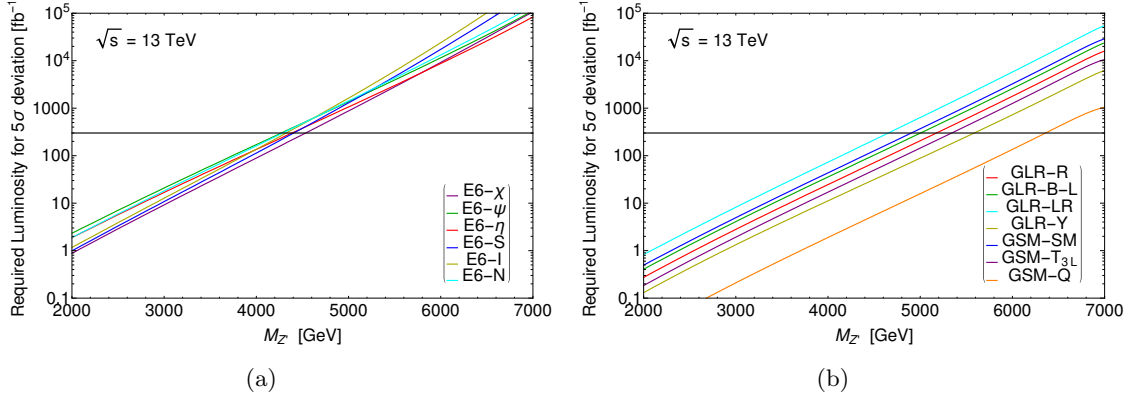
Figure 3. (a) Discovery potential of the 13 TeV LHC for the E_6 class of models. We plot the 5σ contours as a function of Z'-boson mass and luminosity. We perform a combined analysis over e^+e^- and $\mu^+\mu^-$ pairs and assume the $A \times \epsilon$ factor given by CMS at the 8 TeV LHC. (b) Same for the GSM and GLR classes of models.

Figure 4. (a) Exclusion potential of the 13 TeV LHC for the E_6 class of models. We plot the 2σ contours as a function of Z'-boson mass and luminosity. We perform a combined analysis over e^+e^- and $\mu^+\mu^-$ pairs and assume the $A \times \epsilon$ factor given by CMS at the 8 TeV LHC. (b) Same for the GSM and GLR classes of models.
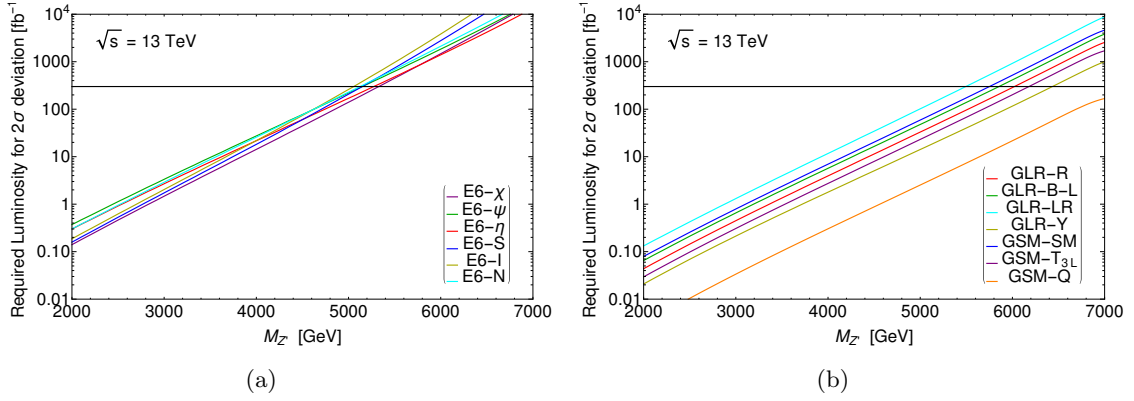
Class	E_6						GLR				GSM		
$U'(1)$ Models	χ	ψ	η	S	I	N	R	$B-L$	LR	Y	SM	T_{3L}	Q
$M_{Z'}$ [GeV]	4535	4270	4385	4405	4325	4290	5175	5005	4655	5585	4905	5340	6360
$M_{Z'}$ [GeV]	5330	5150	5275	5150	5055	5125	6020	5855	5495	6435	5750	6180	8835

Table 2. Projection of discovery limits (first row) and exclusion limits (second row) on the Z'-boson mass from direct searches at the forthcoming Run II of the LHC at 13 TeV. We assume the original design value for the integrated luminosited: $\mathcal{L} = 300\,fb^{-1}$. We consider thirteen different models with an extra $U'(1)$ gauge group predicting a new heavy neutral boson characterized by a narrow width. From left to right, the columns indicate the $M_{Z'}$ limit in GeV within the E_6, GLR and GSM class of models.

for example, [26–28] and references therein). This is not an easy task and the sensitivity of AFB measurements to new physics like additional Z'-bosons has therefore received a lot of attention in the past years. For Drell-Yan processes, AFB is defined from the angular distribution

$$\frac{d\sigma}{d\cos\theta_l} \propto \frac{1}{4\cdot 3}\sum_{\text{spin, col}}\left|\sum_i \mathcal{M}_i\right|^2 = \frac{\hat{s}^2}{12}\sum_{i,j}P_i^* P_j[(1+\cos^2\theta_l)C_S^{ij} + 2\cos\theta_l C_A^{ij}] \qquad (3.1)$$

where θ_l is the lepton angle with respect to the quark direction in the di-lepton center-of-mass frame (CM), which can be derived from the measured four-momenta of the di-lepton system in the laboratory frame. The AFB is indeed given by the coefficient of the contribution to the angular distribution linear in $\cos\theta_l$. In eq. (3.1), $\sqrt{\hat{s}}$ is the invariant mass of the di-lepton system, and P_i and P_j are the propagators of the gauge bosons involved in the process. At tree-level, the Drell-Yan production of charged lepton pairs is mediated by three gauge bosons: the SM photon and Z-boson and the hypothetical Z'-boson. These three vector boson exchanges all participate in the matrix element squared. We thus have:

$$P_{ij} \equiv \text{Re}[P_i^* P_j] = \frac{(\hat{s}-M_i^2)(\hat{s}-M_j^2) + M_i\Gamma_i M_j\Gamma_j}{\left((\hat{s}-M_i^2)^2 + M_i^2\Gamma_i^2\right)\left((\hat{s}-M_j^2)^2 + M_j^2\Gamma_j^2\right)} \qquad (3.2)$$

where M_i and Γ_i are the mass and width of the gauge bosons involved and $i,j = \{\gamma, Z, Z'\}$. Finally, the factors C_S^{ij} and C_A^{ij} in the angular distribution given in eq. (3.1) are coefficients which are functions of the chiral quark and lepton couplings, $q_{L/R}^i$ and $e_{L/R}^i$, to the i-boson with $i = \{\gamma, Z, Z'\}$:

$$C_S^{ij} = (q_L^i q_L^j + q_R^i q_R^j)(e_L^i e_L^j + e_R^i e_R^j), \qquad (3.3)$$
$$C_A^{ij} = (q_L^i q_L^j - q_R^i q_R^j)(e_L^i e_L^j - e_R^i e_R^j). \qquad (3.4)$$

One can conveniently compute the forward (F) and backward (B) contributions to the total cross section integrating over opposite halves of the angular phase space:

$$d\hat{\sigma}_{\text{F}} = \int_0^1 \frac{d\hat{\sigma}}{d\cos\theta_l} d\cos\theta_l = \frac{\hat{s}}{192\pi}\sum_{i,j\geq i}\frac{P_{ij}}{1+\delta_{ij}}\left(\frac{4}{3}C_S^{ij} + C_A^{ij}\right), \qquad (3.5)$$

$$d\hat{\sigma}_{\text{B}} = \int_{-1}^0 \frac{d\hat{\sigma}}{d\cos\theta_l} d\cos\theta_l = \frac{\hat{s}}{192\pi}\sum_{i,j\geq i}\frac{P_{ij}}{1+\delta_{ij}}\left(\frac{4}{3}C_S^{ij} - C_A^{ij}\right), \qquad (3.6)$$

where i and j sum over the mediating resonances, $\{\gamma, Z, Z'\}$.

From the above expressions one can immediately see that the total cross section, $\sigma = \sigma_{\text{F}}+\sigma_{\text{B}}$, depends uniquely on the parity symmetric coefficient C_S. Conversely, the difference between forward and backward cross sections, $\sigma_{\text{F}} - \sigma_{\text{B}}$, preserves only the contribution proportional to the parity antisymmetric coefficient C_A. This is the term which is related to the AFB. One can thus define the AFB as the difference between forward and backward

cross sections normalized to the total cross section:

$$\hat{\sigma} = d\hat{\sigma}_{\mathrm{F}} + d\hat{\sigma}_{\mathrm{B}} = \frac{\hat{s}}{72\pi} \sum_{i,j \geq i} \frac{P_{ij}}{1 + \delta_{ij}} C_S^{ij},$$

$$A_{\mathrm{FB}} = \frac{d\hat{\sigma}_{\mathrm{F}} - d\hat{\sigma}_{\mathrm{B}}}{d\hat{\sigma}_{\mathrm{F}} + d\hat{\sigma}_{\mathrm{B}}} = \frac{\hat{s}}{96\pi\hat{\sigma}} \sum_{i,j \geq i} \frac{P_{ij}}{1 + \delta_{ij}} C_A^{ij}$$

(3.7)

with the SM background corresponding to $ij = \gamma\gamma, ZZ, \gamma Z$ and the new physics given by $ij = \gamma Z', ZZ', Z'Z'$. In the light of the above discussion, the total cross section and AFB depend on different combinations of Z'-boson couplings to ordinary matter. For that reason, the AFB can give complementary information about the structure of such couplings when compared to the total cross section. This feature has motivated several authors to study the potential of the AFB observable in interpreting a possible Z'-boson discovery obtained in the usual resonance hunt as in refs. [26, 27, 29, 30]. Our point is that AFB can also be a powerful tool to search for new physics.

3.1 The reconstructed AFB

The AFB is obtained by integrating the lepton angular distribution forward and backward with respect to the quark direction. As in pp collisions the original quark direction is not known, one has to extract it from the kinematics of the di-lepton system. In this analysis, we follow the criteria of ref. [31] and simulate the quark direction from the boost of the di-lepton system with respect to the beam axis (z-axis). This strategy is motivated by the fact that at the pp LHC the di-lepton events at high invariant mass come from the annihilation of either valence quarks with sea antiquarks or sea quarks with sea antiquarks. As the valence quarks carry away, on average, a much larger fraction of the proton momentum than the sea antiquarks, the boost direction of the di-lepton system should give a good approximation of the quark direction. A leptonic forward-backward asymmetry can thus be expected with respect to the boost direction. In contrast, the subleading number of di-lepton events which originate from the annihilation of quark-antiquark pairs from the sea must be symmetric.

As a measure of the boost, we define the di-lepton rapidity

$$y_{l\bar{l}} = \frac{1}{2} \ln \left[\frac{\mathrm{E} + \mathrm{P_z}}{\mathrm{E} - \mathrm{P_z}} \right]$$

(3.8)

where E and P_z are the energy and the longitudinal momentum of the di-lepton system, respectively. We identify the quark direction through the sign of $y_{l\bar{l}}$. In this way, one can define the reconstructed forward-backward asymmetry, from now on called A_{FB}^*. Namely, we have defined A_{FB}^* using the θ_l^* reconstructed angle, which is the angle between the final state lepton and the incoming quark direction in the center-of-mass of the di-lepton system. As the AFB reconstruction procedure relies on the correlation between the boost variable, $y_{l\bar{l}}$, and the direction of the incoming valence quark, it is therefore more likely to pick up the true direction of the quark for higher values of $y_{l\bar{l}}$. Increasing the probability of identifying the direction of the quark would lead to an observed value of A_{FB}^* that is closer

to the 'true' value of A_{FB} if one were able to access the partonic CM frame. The tradeoff occurs in the reduction of statistics which impacts the significances the other way. The general definition of significance S between predictions of an observable O with uncertainty δO from two hypotheses is

$$S = \frac{|O_1 - O_2|}{\sqrt{\delta O_1^2 + \delta O_2^2}}.$$

The statistical uncertainty on the AFB is given by

$$\delta A_{\text{FB}} = \sqrt{\frac{4}{\mathcal{L}} \frac{\sigma_{\text{F}} \sigma_{\text{B}}}{(\sigma_{\text{F}} + \sigma_{\text{B}})^3}} = \sqrt{\frac{(1 - A_{\text{FB}}^2)}{\sigma \mathcal{L}}} = \sqrt{\frac{(1 - A_{\text{FB}}^2)}{N}},$$

where $\mathcal{L}$ is the integrated luminosity and N the total number of events. One can thus see that the significance is proportional to the root of the total number of events. Imposing a stringent cut on the boost variable, $y_{l\bar{l}}$, would then improve the reconstructed AFB guiding it towards its true line shape, but it will decrease the statistics. In the next subsection, the subtle balance between line shape gain and statistics loss in maximizing the significance via the di-lepton rapidity cut will be discussed in detail.

3.2   On the di-lepton rapidity cut

As discussed in the previous section, since the true quark direction is not known in pp collisions, at the LHC one has to extract it from the kinematics of the di-lepton system. In this paper, the valence quark direction is approximated by the boost direction of the $l^+ l^-$ pairs with respect to the beam axis, that is given by the sign of the di-lepton rapidity $y_{l\bar{l}}$ defined in eq. (3.8). The correctness of this assignment as a function of $y_{l\bar{l}}$ has been studied in ref. [31] for di-lepton events with invariant masses above $400\,\text{GeV}$. In this section, we further analyse this issue by investigating the energy scale dependence of the probability of getting the true quark direction via the sign of $y_{l\bar{l}}$. In figures 5(a) and 5(b), we plot the fraction of events with the correctly assigned direction for up-quarks and down-quarks, respectively, as a function of $|y_{l\bar{l}}|$ for different invariant mass windows of the di-lepton system. The fraction of correctly assigned events increases with the rapidity, confirming the results presented in literature [31]. The additional information contained in figure 5 is that such an increase depends on the energy scale. For di-lepton invariant masses of TeV order the probability of getting the true quark direction becomes more than 80% for a rapidity cut $|y_{l\bar{l}}| \geq 0.8$. For higher invariant masses, beyond the present Z'-boson limits of $O(3\,\text{TeV})$, the same probability can be obtained by imposing a lower rapidity cut: $|y_{l\bar{l}}| \geq 0.35$. Moreover, up-quarks and down-quarks respond differently to the $|y_{l\bar{l}}|$ cut. The probability of getting the correct direction is higher for up-quarks than for down-quarks, at fixed $|y_{l\bar{l}}|$ value. In figure 6, the fraction of correctly assigned events is shown as a function of the invariant mass for five different cuts on the magnitude of the di-lepton rapidity, $|y_{l\bar{l}}|$. This time, we consider the average over up and down-quarks. From here, one can see that, in searching for extra Z'-bosons with masses larger than $O(3\,\text{TeV})$ the $|y_{l\bar{l}}|$ cut is not mandatory. The true direction of the quark is indeed correctly guessed more than 70% of the times, even if no cut is applied on the di-lepton rapidity. This means that, at
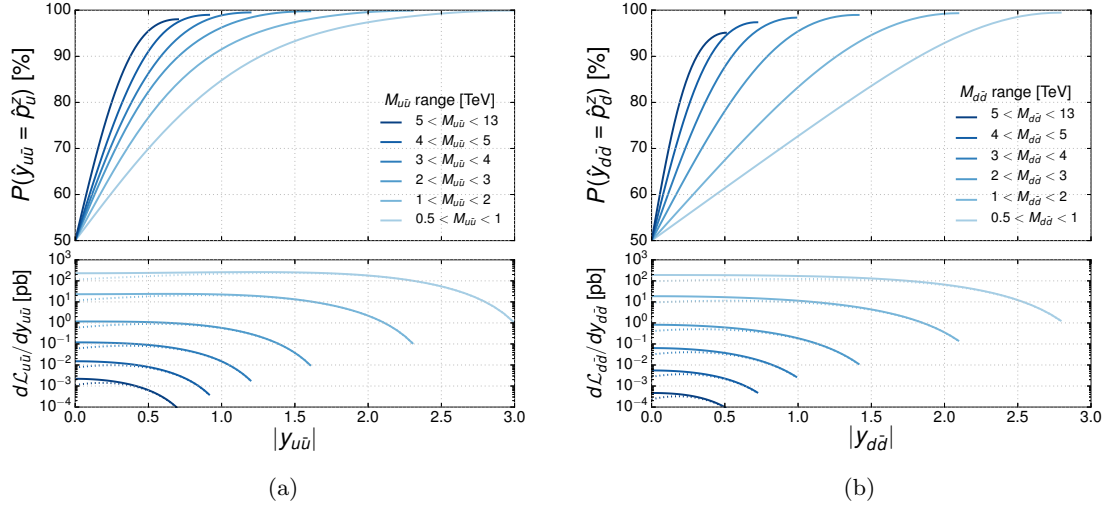
Figure 5. (a) Upper plot: probability of getting the correct direction of the valence up-quark at the 13 TeV LHC via the boost direction of the di-lepton system, given by the sign of the di-lepton rapidity $y_{l\bar{l}}$, as a function of the modulus $|y_{l\bar{l}}| = |y_{u\bar{u}}|$ for six different invariant mass windows scanning from 500 GeV to 5000 GeV and beyond. Lower plot: differential luminosity as a function of $|y_{l\bar{l}}|$ for the correctly assigned quark pair (dashed-line) and for the full sample (solid line). (b) Same as (a) for valence down-quarks.

high di-lepton invariant masses, we should be able to observe a lepton asymmetry with a well approximated shape even without imposing ad hoc cuts. As we discuss in the next two pages, the advantage of not imposing a $|y_{l\bar{l}}|$-cut would be twofold: preserving a small statistical error on that shape, owing to the much larger acceptance one should have in absence of the $|y_{l\bar{l}}|$ cut (see figures 7 and 8), and working with an event sample flavour independent up to a large extent (see figure 8). This latter feature would guarantee a more model independent procedure, as the different Z' models have obviously different couplings of the extra gauge boson to up and down-quarks.

Let us start to clarify these two points. We address first the statistical/acceptance issue. In order to quantify the delicate balance between AFB line shape and statistical error, in the upper plot of figure 7 we show the shape of the reconstructed lepton asymmetry, A_{FB}^*, within the SM as a function of the di-lepton invariant mass for a set of different cuts on $|y_{l\bar{l}}|$. We compare the results to the true AFB, where the direction of the valence quark is taken directly from the Monte Carlo (MC) event generator. In the lower plot of figure 7, we display the acceptance as a function of the same variable $M_{l\bar{l}}$ for the same set of $|y_{l\bar{l}}|$ cuts. Comparing the two plots, one can see that A_{FB}^* tends to the true AFB with increasing the $|y_{l\bar{l}}|$ cut, but at the same time the acceptance heavily decreases. In particular, for masses above 2.5 TeV, if we apply the stringent cut $|y_{l\bar{l}}| \geq 0.8$ used in literature, the number of events goes down by a factor of 3 while the gain in shape is only about 20% of the true AFB value. With increasing mass, the acceptance decreases indeed more rapidly with the $|y_{l\bar{l}}|$ cut.

To visualize how the above features impact the AFB sensitivity to new physics, in figure 8 we compare the reconstructed A_{FB}^* observable predicted by three representative
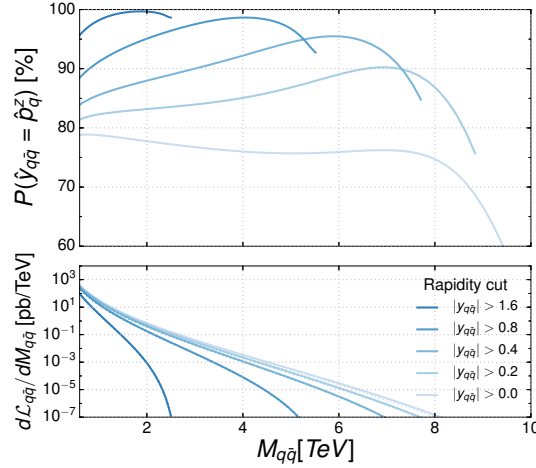
– 13 –

Figure 6. Upper plot: probability of getting the correct direction of the valence quarks at the 13 TeV LHC via the boost direction of the di-lepton system, given by the sign of the di-lepton rapidity $y_{l\bar{l}}$, as a function of the di-quark (or di-lepton) invariant mass for five different cuts on the di-lepton rapidity. Lower plot: differential luminosity as a function of the di-lepton invariant mass for the correctly assigned quark pair (dashed-line) and for the full sample (solid line). Here we average on both up and down-quarks.
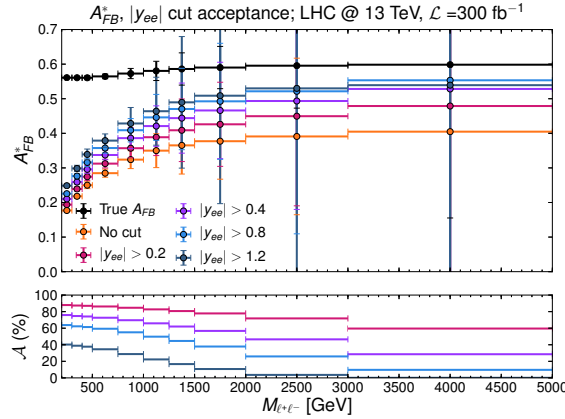

Figure 7. Upper plot: reconstructed forward-backward asymmetry as a function of the di-lepton invariant mass within the SM at the 13 TeV LHC with a total integrated luminosity $\mathcal{L} = 300\,fb^{-1}$ for a set of different rapidity cuts on the di-lepton system. In the legend, $|y_{ee}|$ corresponds to $|y_{l\bar{l}}|$ defined in the text. The black line represents the true AFB for comparison. Lower plot: acceptance as a function of the di-lepton invariant mass for the same set of di-lepton rapidity cuts as above.

Z'-models (E_χ, E_I and GLR–LR) with the SM expectation at the 13 TeV LHC with total integrated luminosity $\mathcal{L} = 100\,fb^{-1}$. As a new physics signal, we consider a hypothetical Z'-boson with mass $M_{Z'} = 3$ TeV. To quantify the effect of the di-lepton rapidity cut on the significance either in searching for new physics via AFB or in distinguishing between different Z' models, we show results for the commonly used $|y_{l\bar{l}}| \geq 0.8$ setup (figure 8(d)) versus the $|y_{l\bar{l}}| \geq 0.4$ (figure 8(c)) and no cut (figure 8(b)) scenarios. We further display, in
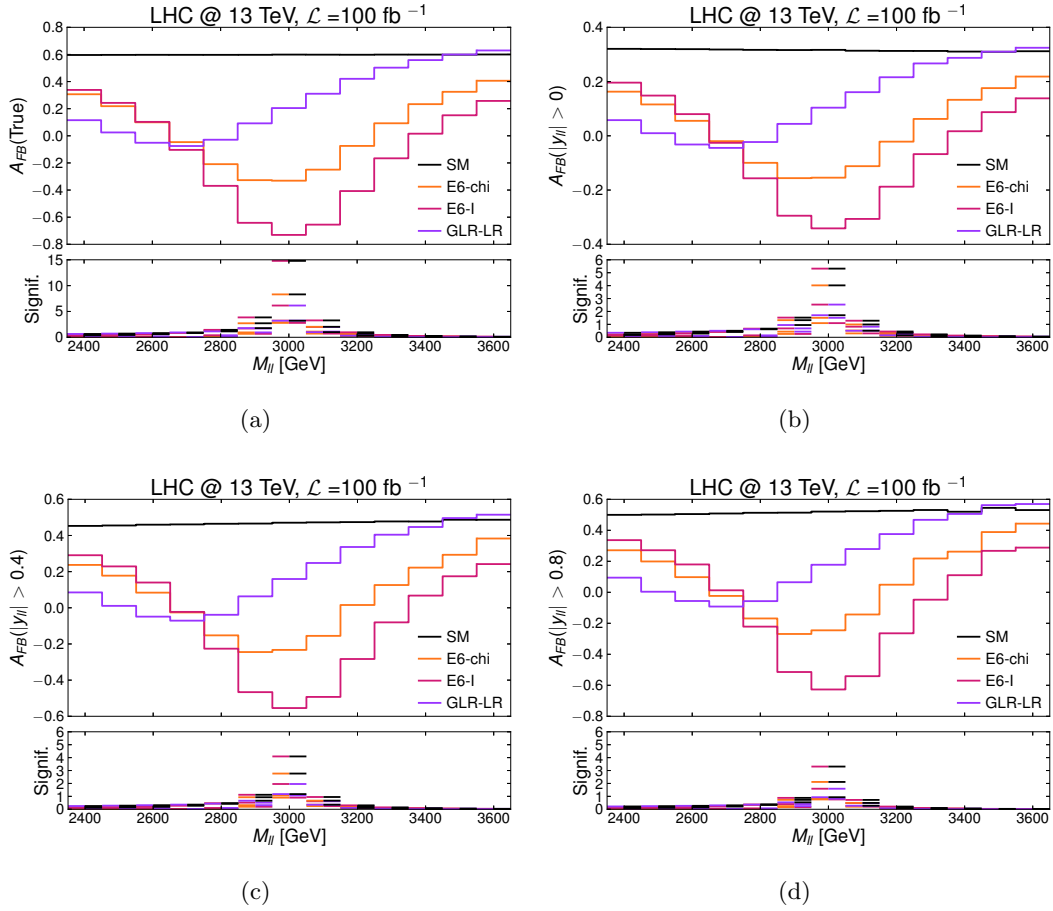
Figure 8. (a) True forward-backward asymmetry as a function of the di-lepton invariant mass as predicted by the SM (black), the E_χ (orange), the E_I (magenta) and the GLR–LR (purple) models for a Z'-boson with mass $M_{Z'} = 3\,\mathrm{TeV}$. The results are for the LHC at $\sqrt{s} = 13\,\mathrm{TeV}$ and $\mathcal{L} = 100\,fb^{-1}$. Lower plot: the significance in distinguishing models is displayed. The double colour in each bin visualizes the two compared models. (b) Reconstructed forward-backward asymmetry as a function of the di-lepton invariant mass as predicted by the SM (black), the E_χ (orange), the E_I (magenta) and the GLR–LR (purple) models for a Z'-boson with mass $M_{Z'} = 3\,\mathrm{TeV}$. The results are for the LHC at $\sqrt{s} = 13\,\mathrm{TeV}$ and $\mathcal{L} = 100\,fb^{-1}$. No cut on the di-lepton rapidity is imposed: $|y_{l\bar{l}}| \geq 0$. Lower plot: the significance in distinguishing models is displayed. (c) Same as plot (b) with $|y_{l\bar{l}}| \geq 0.4$. (d) Same as plot (b) with $|y_{l\bar{l}}| \geq 0.8$.

figure 8(a), the ideal situation represented by the true forward-backward asymmetry, A_{FB}. As one can see, imposing a strong di-lepton rapidity cut helps in recovering the true shape and magnitude of the forward-backward asymmetry. However, the consequent decrease of the number of events is so substantial that the significance diminishes drastically with increasing the $|y_{l\bar{l}}|$ cut.

In addition, and here we address the second point previously anticipated, the implementation of the $|y_{l\bar{l}}|$ cut accentuates the flavour dependence of the results or, in other words, the model dependence of the analysis. As the probability of guessing the correct direction of the quark in the reconstruction procedure of the AFB as a function of the

$|y_{l\bar{l}}|$ cut depends on the type of quark (up and down-quarks react differently to the cut as shown in figure 5), the reconstructed AFB shows an increased model dependence in its response to the $|y_{l\bar{l}}|$ cut. To exemplify this concept, let us take the third bin from the left in figure 8. There (figure 8(a)), the E_χ and E_I models are degenerate as far as the true asymmetry is considered. When we compare the reconstructed asymmetry, we see that the two models are not degenerate any more in that bin. The splitting increases with the $|y_{l\bar{l}}|$ cut, as the two models react differently to such a cut, having different couplings of the corresponding Z'-boson to up- and down-quarks. In order to minimize the presence of model dependent elements in the analysis, it is thus advisable not to include the di-lepton rapidity cut. Hence, in the following. we will be working in a setup where we do not impose such a restriction.

4 The role of AFB in Z' searches: narrow heavy resonances

The AFB is the observable where the effects of the interference between new physics and SM background are maximal. In the Drell-Yan processes, these effects are of course present also in the total cross section. They are readily seen in both cases in the di-lepton invariant mass. As mentioned repeatedly, constraining the search window for new physics within the interval $|M_{l\bar{l}} - M_{Z'}| \leq 0.05 \times E_{\text{LHC}}$ guarantees that finite width and interference effects are below the $O(10\%)$ level when compared to the complete new physics signal. Such effects are instead an intrinsic part of the AFB and dominate its dynamics. For such a reason, the AFB is an intrinsically model dependent variable and in literature has therefore been traditionally considered for disentangling different models predicting a spin-1 heavy neutral particle. Its role has therefore been cornered so far to the interpretation of a possible Z'-boson discovery obtained via the default bump search.

In this paper, we aim to show that AFB can also be used for searches, directly, as a primary variable alongside the cross section itself. In this section we focus on Z'-bosons characterized by a narrow width. This is the most common kind of particle predicted by theories with an extra $U'(1)$ gauge group. This is also the scenario mostly studied in literature. The experimental searches for such an object are tailored on this expectation and the corresponding results coming from the data collected at the 8 TeV LHC have been summarized in section 2. With respect to the 'AFB search', the Z' models can be divided into two categories: Z' models with AFB centred on the Z'-boson mass and Z' models with shifted AFB. In the next two subsections, we discuss their properties in turn.

4.1 Z' models with AFB centred on peak

In this subsection, we discuss models where the AFB is peaked on the Z'-boson mass. These models belong to the E_6 class of theories which predict new narrow width spin-1 resonances. In the literature, it is known that such models contain one extra neutral gauge boson whose width cannot exceed a few percent of its mass: $\Gamma_{Z'}/M_{Z'} \leq 5\%$. Even the inclusion of new Z'-boson decay channels into exotic states would not change this estimate.

We first compare the shape of the AFB distribution as a function of the di-lepton invariant mass, $M_{l\bar{l}}$, with the differential cross section in the same variable. In figure 9,
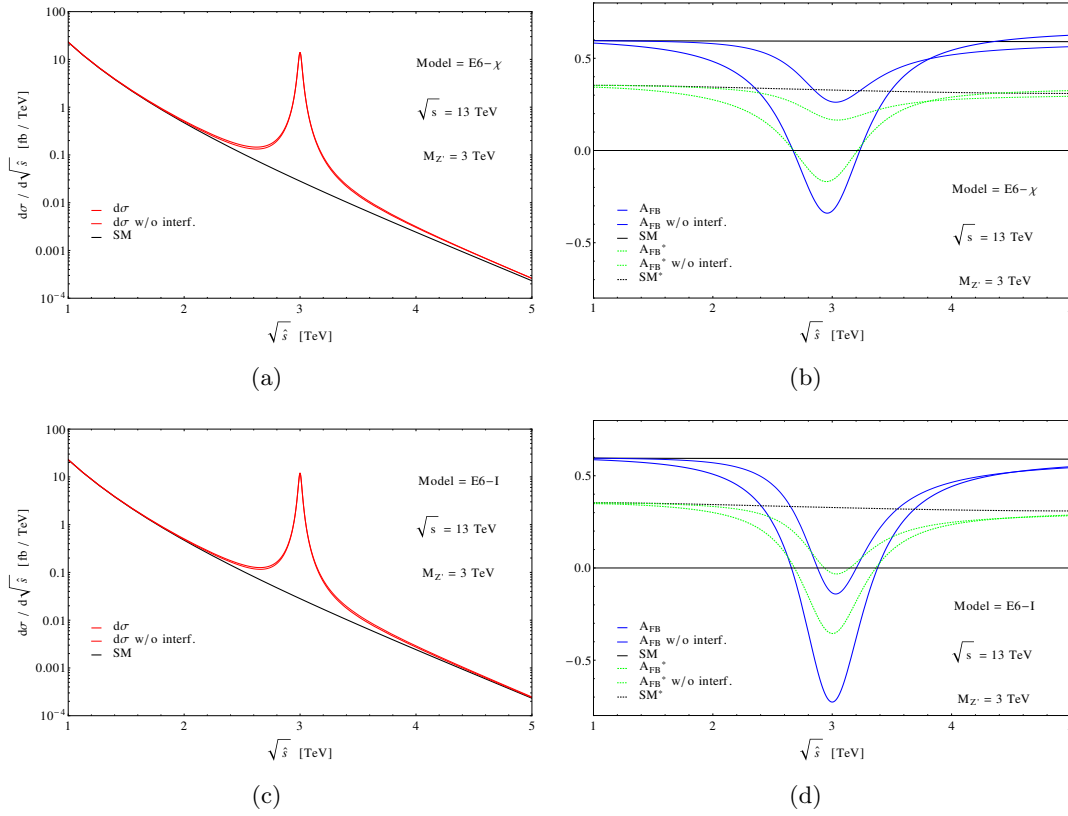
Figure 9. (a) Differential cross section as a function of the di-lepton invariant mass as predicted by the E_χ model for a Z'-boson with mass $M_{Z'} = 3\,\mathrm{TeV}$. The results are for the LHC at $\sqrt{s} = 13\,\mathrm{TeV}$. (b) Reconstructed forward-backward asymmetry as a function of the di-lepton invariant mass as predicted by the E_χ model for a Z'-boson with mass $M_{Z'} = 3\,\mathrm{TeV}$. The results are for the LHC at $\sqrt{s} = 13\,\mathrm{TeV}$. No cut on the di-lepton rapidity is imposed: $|y_{l\bar{l}}| \geq 0$. (c) Same as plot (a) within the E_I model. (d) Same as plot (b) within the E_I model.

we show results for two representative E_6 models: E_χ and E_I. We consider a hypothetical Z'-boson with mass $M_{Z'} = 3\,\mathrm{TeV}$. In figures 9(b) and 9(d), we display both the true and the reconstructed AFB within the two chosen E_6 models with and without taking into account the interference between the extra Z'-boson and the SM background. As one can see, the role played by the interference is extremely important. The AFB shape is drastically modified by getting its peak heavily accentuated. In contrast, the invariant mass distribution is almost interference free if the $|M_{l\bar{l}} - M_{Z'}| \leq 0.05 \times E_{\mathrm{LHC}}$ cut is imposed, as shown in figures 9(a) and 9(c) for the two representative E_6 models. In interpreting the experimental data coming from AFB measurements it is then mandatory to include the interference, no matter what kinematical cut is applied.

In terms of significance, the search for narrow width Z' models with AFB centred on the Z' mass is summarized in figure 10 for the two representative models E_χ and E_I. Within the E_χ model, the true AFB would give rise to a significance slightly lower than that one coming from the usual bump search, as shown in figure 10(a). The reconstruction procedure of the AFB depletes this result but still the two significances from cross section
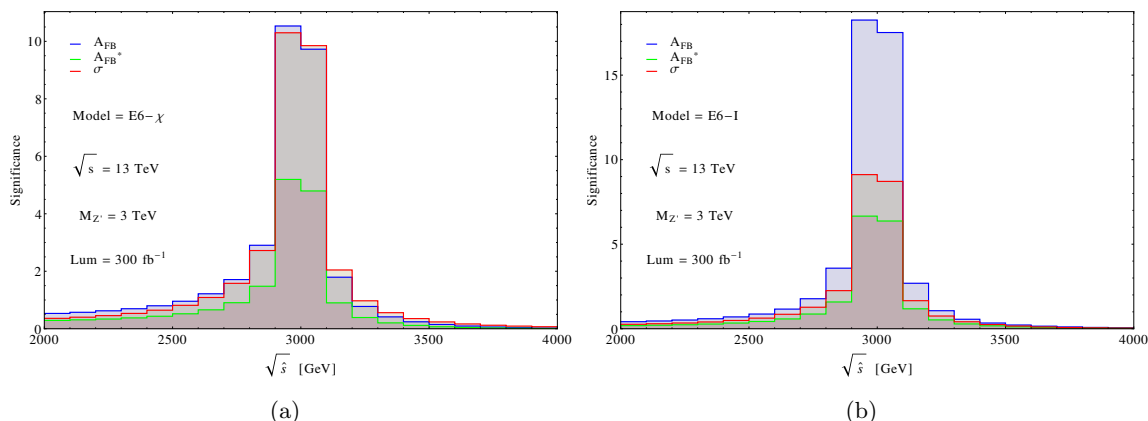
Figure 10. (a) Binned significance as a function of the di-lepton invariant mass as predicted by the E_χ model for a Z'-boson with mass $M_{Z'} = 3\,\text{TeV}$. The red line represents the significance corresponding to the invariant mass distribution. The blue and green lines show the significance extracted by an ideal measurement of true and reconstructed AFB, respectively. The results are for the LHC at $\sqrt{s} = 13\,\text{TeV}$ and $\mathcal{L} = 300\,fb^{-1}$. (b) Same as (a) for the E_I model.

and A_{FB}^* are comparable over the full di-lepton invariant mass range. Figure 10(b) shows that the E_I model is more accessible through the AFB than the cross section. There, indeed, the significance from the true AFB is a factor two bigger than the significance coming from the bump search. Once again, the AFB reconstruction pollutes the ideal result. The significance from the reconstructed AFB gets reduced, but its value remains anyhow only slightly lower than that one coming from the resonance search. The E_I model is not unique in this respect, also the E_S model shares the same property.

Similar trends are shown by all models belonging to the E_6 class of theories and do not change when a more realistic setup is considered. Implementing the acceptance cuts extracted by the CMS analysis at the 8 TeV LHC ($P_T(l) \geq 25\,\text{GeV}$ and $\eta(l) \leq 2.5$ with $l = e, \mu$), the shape of the reconstructed AFB, A_{FB}^*, including error bars would in fact appear as in figure 11. The significances coming from the AFB and the cross section are indeed equivalent in magnitude, if only the statistical error is included. We thus expect that the use of the A_{FB}^* observable, when associated to the default resonance search, could improve the discovery potential of new narrow width Z'-bosons. Further, being a ratio of differential cross sections, the reconstructed A_{FB}^* could help in minimizing the systematical errors thus rendering the measurement much more accurate.

This is in particular the case when we should be in presence of an evidence for a new Z'-boson in the resonance search at the 3–4 sigma level. In these conditions, one could not claim the discovery of a new gauge boson just looking at the resonant peak in the di-lepton invariant mass distribution. However, if a signal of similar strength were to be discovered in an independent observable, the suggestion of the possible presence of new physics would turn into a robust claim. This is the role that the AFB would play. In figure 12, we plot the differential cross section and A_{FB}^* as a function of in the di-lepton invariant mass, $M_{l\bar{l}} = \sqrt{\hat{s}}$, within the E_χ and E_I models, at the forthcoming Run II of the LHC at 13 TeV with $\mathcal{L} = 30\,fb^{-1}$, that is the integrated luminosity which should be collected at the end
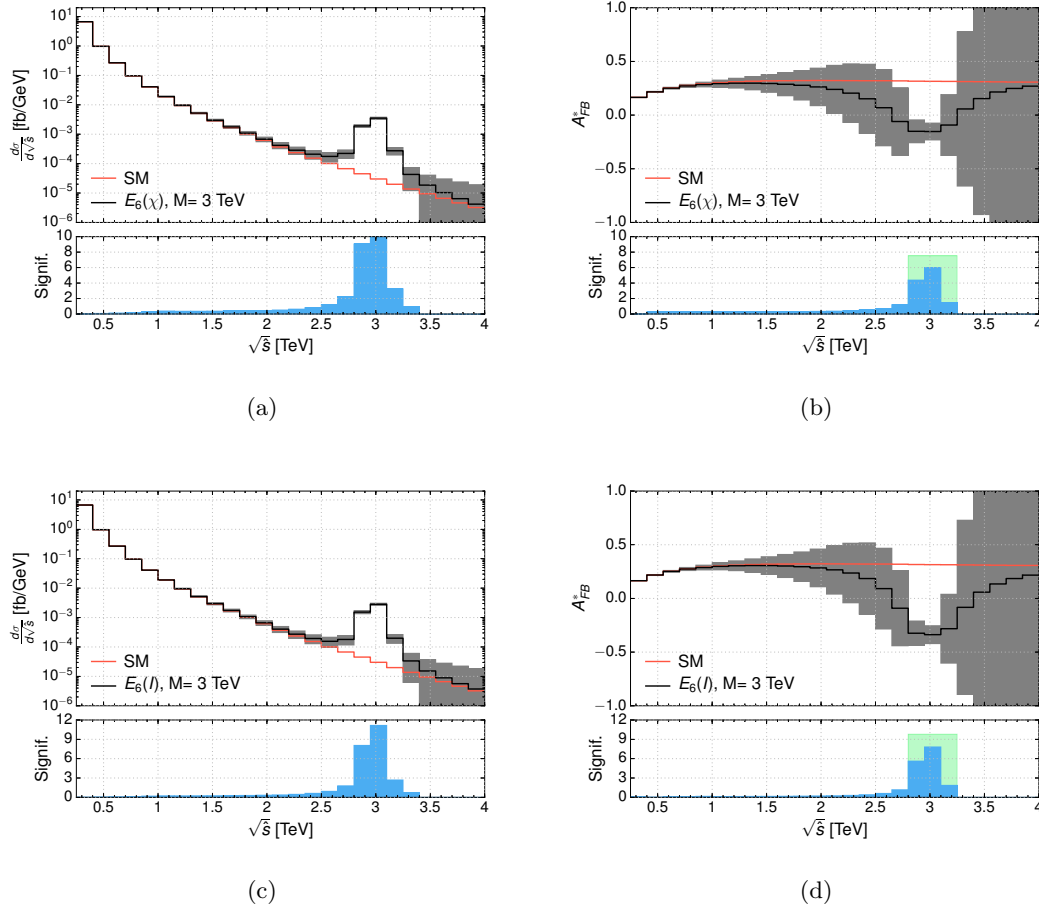
(a)

(b)

(c)

(d)

Figure 11. (a) Binned differential cross section as a function of the di-lepton invariant mass within the E_χ model for a Z'-boson with mass $M_{Z'} = 3\,\text{TeV}$. Error bars are included. The results are for the LHC at $\sqrt{s} = 13\,\text{TeV}$ and $\mathcal{L} = 300\,fb^{-1}$. Acceptance cuts are imposed (see text). The lower plot shows the significance. (b) Binned A^*_{FB} as a function of the di-lepton invariant mass within the E_χ model for a Z'-boson with mass $M_{Z'} = 3\,\text{TeV}$. Error bars are included. The results are for the LHC at $\sqrt{s} = 13\,\text{TeV}$ and $\mathcal{L} = 300\,fb^{-1}$. Acceptance cuts are imposed (see text). In the lower plot, the blue histogram shows the binned significance while the green area indicates the total significance integrated over that invariant mass region. (c) Same as (a) for the E_I model. (d) Same as (b) for the E_I model.

of 2016. There, a new physics evidence at barely 4 sigma in the bump search could be reinforced by the simultaneous measurement of the reconstructed AFB, showing a signal at the 2-sigma level.

4.2 Z' models with shifted AFB

In this section, we discuss narrow width Z' models where the AFB has a shifted peak, that is, not centred on the Z'-boson mass. These models belong to the GLR class. The same behaviour is also displayed by the SSM scenario taken as benchmark model by the LHC experimental collaborations.
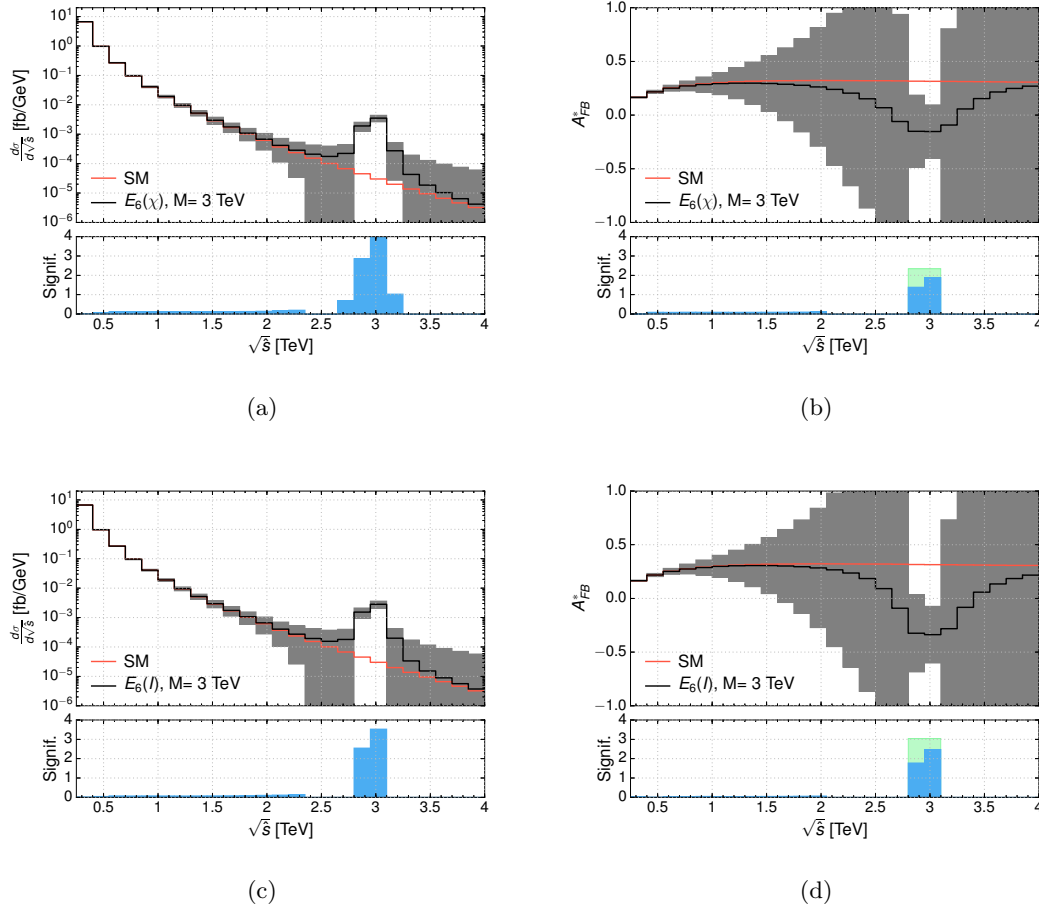
Figure 12. (a) Binned differential cross section as a function of the di-lepton invariant mass as predicted by the E_χ model for a Z'-boson with mass $M_{Z'} = 3\,\mathrm{TeV}$. Error bars are included. The results are for the LHC at $\sqrt{s} = 13\,\mathrm{TeV}$ and $\mathcal{L} = 30\,fb^{-1}$. Acceptance cuts are imposed (see text). The lower plot shows the significance. (b) Binned A^*_{FB} as a function of the di-lepton invariant mass as predicted by the E_χ model for a Z'-boson with mass $M_{Z'} = 3\,\mathrm{TeV}$. Error bars are included. The results are for the LHC at $\sqrt{s} = 13\,\mathrm{TeV}$ and $\mathcal{L} = 30\,fb^{-1}$. Acceptance cuts are imposed (see text). In the lower plot, the blue histogram shows the significance bin by bin while the green area indicate the total significance integrated over that invariant mass region. (c) Same as (a) for the E_I model. (d) Same as (b) for the E_I model.

In principle, the reconstructed A^*_{FB} could reveal the presence of a new spin-1 particle at energy scales lower than its mass, as the shape of this observable as a function of the di-lepton invariant mass is accentuated at mass scales smaller than $M_{Z'}$. This behaviour is shown in figure 13(b) where we plot the reconstructed AFB versus $M_{l\bar{l}} = \sqrt{\hat{s}}$ for the representative model GLR–LR. We consider a new Z'-boson with mass $M_{Z'} = 3\,\mathrm{TeV}$. As one can see, the peak of A^*_{FB} is shifted on the left-hand side of the physical Z'-boson mass and it appears at around $2.6\,\mathrm{TeV}$. This feature is interesting. However, the significance is quite low as shown in figure 13(b), owing to the poor statistics in that region. For $M_{l\bar{l}}$ values around the physical mass of the Z'-boson, which are statistically relevant, the
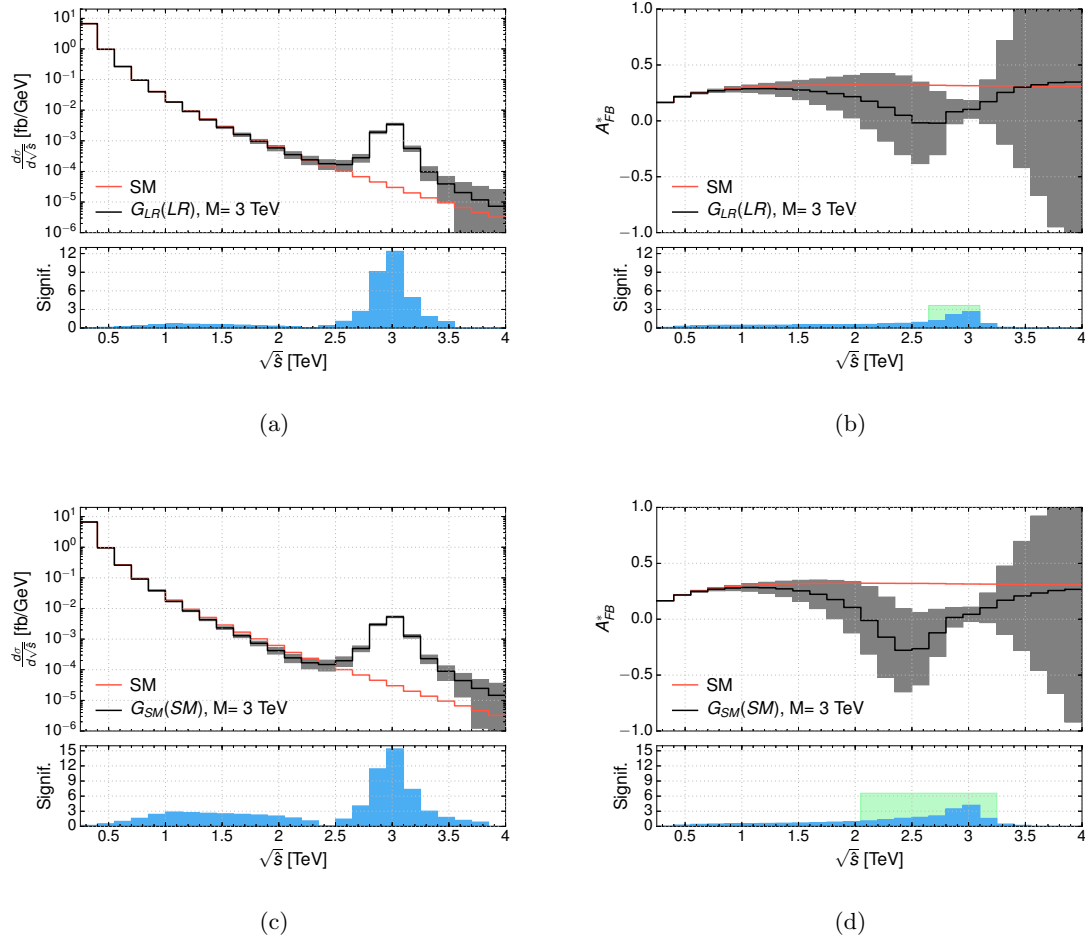
Figure 13. (a) Binned differential cross section as a function of the di-lepton invariant mass as predicted by the GLR–LR model for a Z'-boson with mass $M_{Z'} = 3\,\mathrm{TeV}$. Error bars are included. The results are for the LHC at $\sqrt{s} = 13\,\mathrm{TeV}$ and $\mathcal{L} = 300\,fb^{-1}$. Acceptance cuts are included (see text). (b) Binned A^*_{FB} as a function of the di-lepton invariant mass as predicted by the GLR–LR model for a Z'-boson with mass $M_{Z'} = 3\,\mathrm{TeV}$. Error bars are included. The results are for the LHC at $\sqrt{s} = 13\,\mathrm{TeV}$ and $\mathcal{L} = 300\,fb^{-1}$. Acceptance cuts are included (see text). (c) Same as (a) for the Generalized Sequential SM, GSM–SM. (d) Same as (b) for the GSM–SM model.

significance coming from AFB is always much smaller than the significance obtained via the measurement of the differential cross section, displayed in figure 13(a). For these kind of models, the A^*_{FB} observable is therefore not particularly appropriate for Z' searches. The same conclusion holds for the SSM (see figures 13(c) and 13(d)). Hence, this benchmark model is not an advisable playground for studying the benefits of using the AFB in searching for new Z'-bosons.

5 The role of AFB in Z' searches: wide heavy resonances

In this section, we discuss the role of the reconstructed AFB, A^*_{FB}, in searches for a new Z'-boson characterized by a large width. Such a heavy and wide particle is predicted by
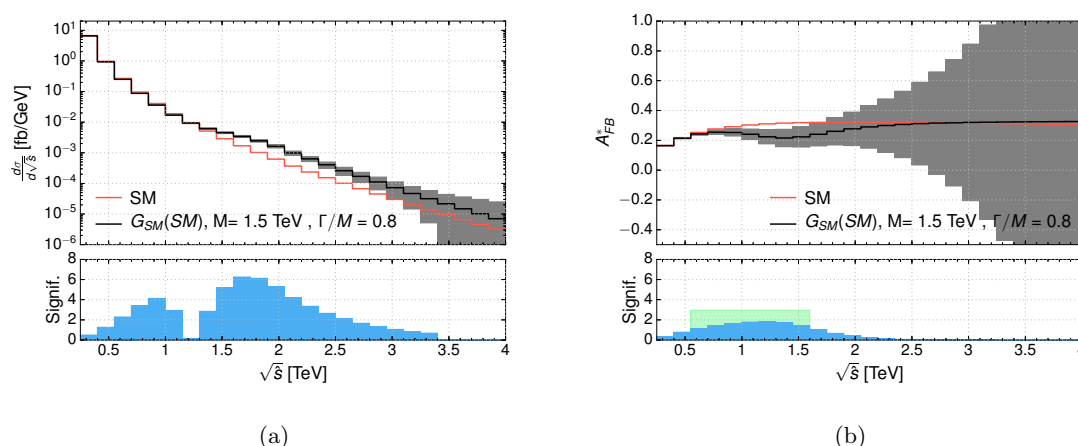
Figure 14. (a) Binned differential cross section as a function of the di-lepton invariant mass as predicted by the GSM–SM model for a Z'-boson with mass $M_{Z'} = 1.5\,\text{TeV}$ and $\Gamma_{Z'}/M_{Z'} = 80\%$. Error bars are included. The results are for the LHC at $\sqrt{s} = 13\,\text{TeV}$ and $\mathcal{L} = 300\,fb^{-1}$. Acceptance cuts are included (see text). (b) Binned A^*_{FB} as a function of the di-lepton invariant mass as predicted by the GSM–SM model for a Z'-boson with mass $M_{Z'} = 1.5\,\text{TeV}$ and $\Gamma_{Z'}/M_{Z'} = 80\%$. Error bars are included. The results are for the LHC at $\sqrt{s} = 13\,\text{TeV}$ and $\mathcal{L} = 300\,fb^{-1}$. Acceptance cuts are imposed (see text).

different models. A benchmark scenario for experimental analyses is the wide version of the SSM described in ref. [10]. The proposal is to have a heavy copy of the SM neutral gauge boson, Z, with same couplings to ordinary matter and SM gauge bosons. Owing to the Z'-boson decay into SM charged gauge bosons, whose rate grows with the third power of the Z'-boson mass, the total width of the new heavy particle can be in principle quite large: $\Gamma_{Z'}/M_{Z'} \simeq 50\%$ and above. In reality, a word of caution should be spent at this point. The triple $Z'WW$ coupling is governed by the mixing of the extra Z' with the SM Z-boson. The actual size of this $Z - Z'$ mixing is strongly constrained by the ElectroWeak Precision Tests (EWPT), see ref. [3] for a review on these bounds. In this paper, we neither address this issue nor the validity of the wide SSM. We simply take this model as a popular framework that is representative of a wide Z'-boson. In this context, we thus consider the Z' width as a free parameter.

Under this assumption and for a $\Gamma_{Z'}/M_{Z'}$ ratio of several tens of percent, the invariant mass distribution of the two final state leptons does not show in the cross section a resonant (or peaking) structure around the physical mass of the Z'-boson standing sharply over a smooth background, but just a shoulder spread over the SM background. This result is plotted in figure 14(a), where we consider a Z'-boson with mass $M_{Z'} = 1.5\,\text{TeV}$ and width $\Gamma_{Z'}/M_{Z'} = 80\%$. As the line shape of the resonance is not well defined and these parton level results could be worsened by detector smearing effects giving rise to an even broader spectrum, the A^*_{FB} observable could help to interpret a possible excess of events. The results are shown in figure 14(b). There, one can see that the A^*_{FB} shape could be visible at the 2σ level.

A framework, theoretically more grounded than the wide SSM, which predicts a heavy and broad Z'-boson is the so-called non-universal SU(2) model [8, 9]. In this theory, the

third generation of fermions is subjected to a new SU(2) dynamics different from the usual interaction advocated by the SM. On the contrary, the first two families of fermions only feel the SM weak interaction. Owing to the non universality of the gauge interactions, different consequences appear in this model. The CKM matrix is not unitary anymore, although the unitarity violation is suppressed by the heavy scale of the new physics. Also, Flavour Changing Neutral Currents (FCNCs) can generally show up. In addition and of primary interest for this paper, a new spectrum of gauge bosons emerges in the model. These new vector bosons can be either narrow or wide. The only constraint on the model parameters comes from the EWPTs which bound the Z'-boson to have a mass $M_{Z'} \geq 1.7 \, \text{TeV}$. The constraints on mass and couplings of the heavy Z' boson are actually correlated. Usually, they are presented as a two-dimensional contour plot. For the details of the analysis of direct and indirect limits on this model we refer to [9] and references therein.

Within this framework, we consider the wide Z'-boson case with $M_{Z'} = 5.5 \, \text{TeV}$ and $\Gamma_{Z'}/M_{Z'} = 20\%$. This setup fulfills both the limits quoted in ref. [9] and the direct limits coming from direct searches at the 8 TeV LHC [16]. The latter analysis performed at the LHC has been optimized for searches of new physics with no resonant peaking structure. The outcome is that there are no events for di-lepton invariant masses above 1.8 TeV. We have taken this limit into account when evaluating the Z'-boson mass and width.

This model is a very good playground to test whether the AFB can be used as a primary variable in searches for wide objects. In this case, in fact, the new physics signal appears as an excess of events spread over the SM background. Almost no line shape is present in the di-lepton invariant mass distribution usually measured. Searches are performed relying on a pure counting strategy, a procedure which does not allow much interpretation of the hypothetical signal. The exploitation of the reconstructed A_{FB}^* could help in this respect.

In figure 15, we compare the Z'-boson spectrum (15(a)) and the reconstructed A_{FB}^* (15(b)) as functions of the di-lepton invariant mass. As one can see in figure 15(a), the cross section spectrum at parton level is already very broad. Its slope might be lost or mistaken in the SM background normalization. Even if, in the best case, a plateau would be visible over the SM background, its interpretation would be very difficult. The same degree of difficulty would appear in interpreting the depletion of events in the low invariant mass region. In principle such a depletion, due to the negative interference between the extra Z'-boson and the SM background, could give rise to a huge significance as shown in figure 15(a) (lower plot). However, the experimental fitting procedure for this kind of scenarios is not fully settled yet. Severe uncertainties could affect the functional form chosen to simulate the SM background in the data-driven approach, as the new physics effects might invade the low mass spectrum that is instead commonly assumed to be new physics free. The same would happen for the alternative procedure based on the Monte Carlo (MC) estimate of the SM background, as this approach relies on the normalization of the MC prediction to the data around the peak of the SM Z-boson and on the existence of a new physics free control region at low invariant masses. Moreover, even in the ideal case in which all errors were under control, the interpretation of such evidence would be quite complicated, having no defined shape at all. In this context, the Forward-Backward Asymmetry can be of some help. Figure 15(b) shows that the A_{FB}^* observable has a sharper
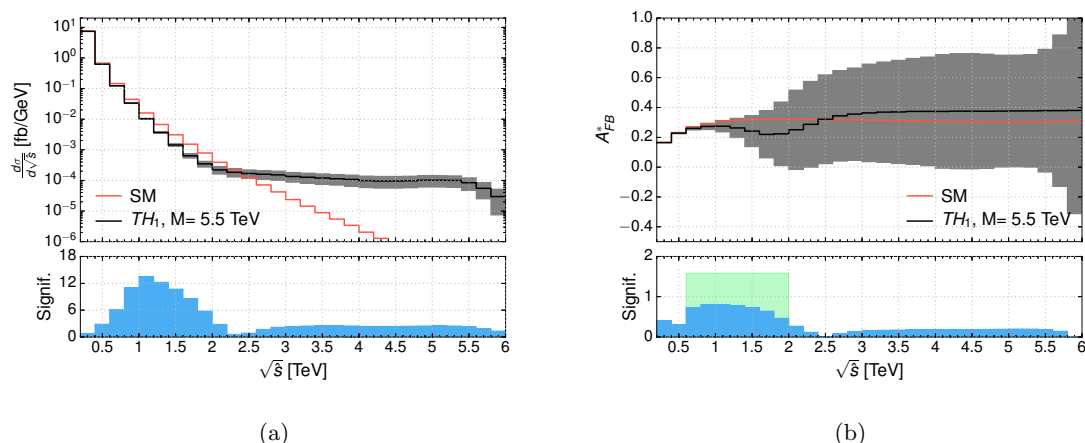
Figure 15. (a) Binned differential cross section as a function of the di-lepton invariant mass as predicted by the non-universal SM (NU SM) for a Z'-boson with mass $M_{Z'} = 5.5\,\text{TeV}$ and $\Gamma_{Z'}/M_{Z'} \simeq 20\%$. Error bars are included. The results are for the LHC at $\sqrt{s} = 13\,\text{TeV}$ and $\mathcal{L} = 300\,fb^{-1}$. Acceptance cuts are imposed (see text). (b) Binned A^*_{FB} as a function of the di-lepton invariant mass as predicted by the NU SM for a Z'-boson with mass $M_{Z'} = 5.5\,\text{TeV}$ and $\Gamma_{Z'}/M_{Z'} \simeq 20\%$. Error bars are included. The results are for the LHC at $\sqrt{s} = 13\,\text{TeV}$ and $\mathcal{L} = 300\,fb^{-1}$. Acceptance cuts are imposed (see text).

line-shape which can reveal the presence of a spin-1 particle beyond error bars. Such a shape is quite shifted at low energy scales though, compared to the Z'-boson mass. Hence, its extraction should enable one to help the discovery of a new vector boson with very high mass. In short, here, the AFB measurement could become particularly useful at the edge of the LHC discovery limits, when new particles can be too heavy and broad to be easily detected via a standard resonant peak search.

The aforementioned scenarios are in fact particularly challenging for experimentalists. The non-resonant analyses of wide objects have been performed by searching for a smooth deviation from the SM background. The number of events above a given lower cut on the di-lepton invariant mass is compared with the total number of expected background events. An optimal minimum mass threshold is chosen to maximize the sensitivity to new physics. Clearly, such an analysis depends quite strongly on the SM background estimate. Usually, the simulated background is normalized to the event number in a mass window of $\pm 30\,\text{GeV}$ around the Z-boson mass. A control region is then selected at higher di-lepton invariant masses in order to perform a data driven modelling of the SM background and recast it in a functional form easy to implement in the likelihood used for extracting the limit on the Z'-boson mass. The method is based on the assumption that the control region is new physics free. But, this is not the case for wide Z'-bosons. In these scenarios, the interference between the extra Z'-boson and the SM γ, Z is so sizeable that it can invade the control region. Being absolutely model-dependent, it can be either constructive or destructive. In any case, it would change accordingly the shape of the di-lepton spectrum. If the interference is negative, it would led to a depletion of events at low mass scales on the left-hand side of the Z'-boson resonance. This is exactly the example shown in figures 14

and 15 corresponding to the SSM and non-universal SU(2) scenarios, respectively. If not correctly interpreted, these interference effects could induce one to underestimate the SM background with the consequence of overestimating the extracted mass bounds. Having all these uncertainties to deal with, the support of a second observable like the AFB is strongly recommended for the non-resonant analyses.

6 On the robustness of AFB against PDF uncertainties

In this section, we discuss how robust the shape of the forward-backward asymmetry is against the theoretical uncertainties on the PDFs. We further compare the systematic error induced by the PDF uncertainty on the differential cross section and on the reconstructed AFB.

For the determination of the PDF uncertainty we follow [32] and references therein. Here, we just highlight the key points of the procedure. We compute the Hessian PDF uncertainty for our two observables: di-lepton invariant mass distribution and reconstructed AFB. For Hessian PDF sets, both a central set and error sets are given. The number of error sets is twice the number of eigenvectors. For the CTEQ6.6 PDF that we use, the number of error sets is equal to 40. For a given observable X we define $X_i^{\pm}$ to be the value of the variable using the PDF error set corresponding to the "$\pm$" direction for the eigenvector i. The symmetric error on the variable X is then given by:

$$\Delta X = \frac{1}{2}\sqrt{\sum_{i=1}^{N} |X_i^+ - X_i^-|^2}.$$ (6.1)

With this definition, we are now ready to compute the PDF uncertainty on any observable X or any function $f(X)$. For the differential cross section, $X = \sigma$, we can thus apply eq. (6.1) directly. For the forward-backward asymmetry, the computation is slightly more involved since AFB is a ratio of (differential) cross sections. In this case, we consider as independent variables the forward and backward (differential) cross sections, σ_{F} and σ_{B}, so that the observable $A_{\mathrm{FB}}^* = f(\sigma_{\mathrm{F}}, \sigma_{\mathrm{B}})$. According to eq. (6.1), the PDF uncertainty on σ_{F} and σ_{B} is given by:

$$\Delta\sigma_{\mathrm{F}} = \frac{1}{2}\sqrt{\sum_{i=1}^{N} |\sigma_{\mathrm{F}i}^+ - \sigma_{\mathrm{F}i}^-|^2}\,; \qquad \Delta\sigma_{\mathrm{B}} = \frac{1}{2}\sqrt{\sum_{i=1}^{N} |\sigma_{\mathrm{B}i}^+ - \sigma_{\mathrm{B}i}^-|^2}.$$ (6.2)

In the Hessian approach, the correlation of the PDF degrees of freedom of any two independent observables, X and Y, is expressed by the quantity $\cos\phi$ given in ref. [32] and reported here below:

$$\cos\phi = \frac{1}{4\Delta X \Delta Y}\sum_{i=1}^{N} (X_i^+ - X_i^-)(Y_i^+ - Y_i^-).$$ (6.3)

The quantity $\cos\phi$ characterizes whether the PDF degrees of freedom of X and Y are partially or fully correlated ($\cos\phi = 1$), fully anti-correlated ($\cos\phi = -1$) or uncorrelated

$(\cos\phi = 0)$. Such a quantity enters in the definition of the PDF uncertainty on any function of two variables, $\Delta f(X, Y)$, as shown in the formula here below (see also ref. [32]):

$$\Delta f(X, Y) = \sqrt{(\Delta X \partial_X f)^2 + 2\Delta X \Delta Y \cos\phi \partial_X f \partial_Y f + (\Delta Y \partial_Y f)^2}. \qquad (6.4)$$

In our case, we have verified that the two independent observables, $X = \sigma_{\mathrm{F}}$ and $Y = \sigma_{\mathrm{B}}$, are fully correlated for all analyzed Z' models ($\cos\phi(\sigma_{\mathrm{F}}, \sigma_{\mathrm{B}}) = 1$) being evaluated at the same energy scale when computing A^*_{FB} as a function of the di-lepton invariant mass. Under this condition, by applying the error chain rule as in eq. (6.4), we get

$$\Delta A^*_{\mathrm{FB}} = \frac{1}{2}(1 - A^*_{\mathrm{FB}}{}^2) \left| \frac{\Delta\sigma_{\mathrm{F}}}{\sigma_{\mathrm{F}}} - \frac{\Delta\sigma_{\mathrm{B}}}{\sigma_{\mathrm{B}}} \right|. \qquad (6.5)$$

The sign appearing in the above formula is crucial for the AFB. It indeed clearly shows that there is a partial cancellation of the PDF error on the reconstructed A^*_{FB} due to the fact that this observable is a ratio of (differential) cross sections. Compared to the differential cross section, the AFB is then more robust against PDF uncertainties. This is shown in figure 16 where we compare the effect of PDF and statistical errors on the shape of the di-lepton invariant mass distribution of the cross section and AFB for two reference models, E_I and E_χ. As one can see, the behaviours of cross section and AFB are opposite. The differential cross section in the di-lepton invariant mass is dominated by the PDF error on-peak and in the low invariant mass region. In the region around the peak and for invariant masses below the TeV region, the PDF uncertainty is a factor 2 bigger than the statistical error. On the contrary, the AFB is always dominated by the statistical error: on and off-peak. Moreover, the PDF uncertainty is quite reduced owing to the minus sign in eq. (6.5). The shape of the AFB is thus not affected by the PDF error, so this observable is theoretically well defined.

In the light of these results, we can revisit figures 11 and 12 which compare differential cross section and AFB for two representative E_6 models and for two luminosity regimes: $\mathcal{L} = 300\,fb^{-1}$ and $\mathcal{L} = 30\,fb^{-1}$ respectively. These two regimes are representative of the next two years data taking ($\mathcal{L} = 30\,fb^{-1}$) and of the design high luminosity Run II ($\mathcal{L} = 300\,fb^{-1}$). We stated previously that in the low luminosity regime the AFB could help interpreting the data. As illustrated in figure 12, the AFB significance could be in fact comparable to that found using the cross section from a binned mass distribution. In case of an early discovery with a few events, the evidence of new physics from the bump search alone would be insufficent to demonstrate the presence of a new Z'. But, it could be reinforced by a further comparable evidence in the independent variable A^*_{FB}, leading to a much more robust result.

The role of AFB in searching for new Z'-bosons is not confined to support a not fully convincing evidence in the usual bump search at low statistics. In this section, the main message is that, even after the high luminosity objective is achieved for the current LHC Run II, the AFB may provide additional evidence of new physics and be very useful in the interpretation of the origin of this new physics. As stated above, this time the reason is the PDF's uncertainty which will dominate the theoretical error on the prediction of a new Z'-boson appearing as a resonant peak in the di-lepton invariant mass distribution.
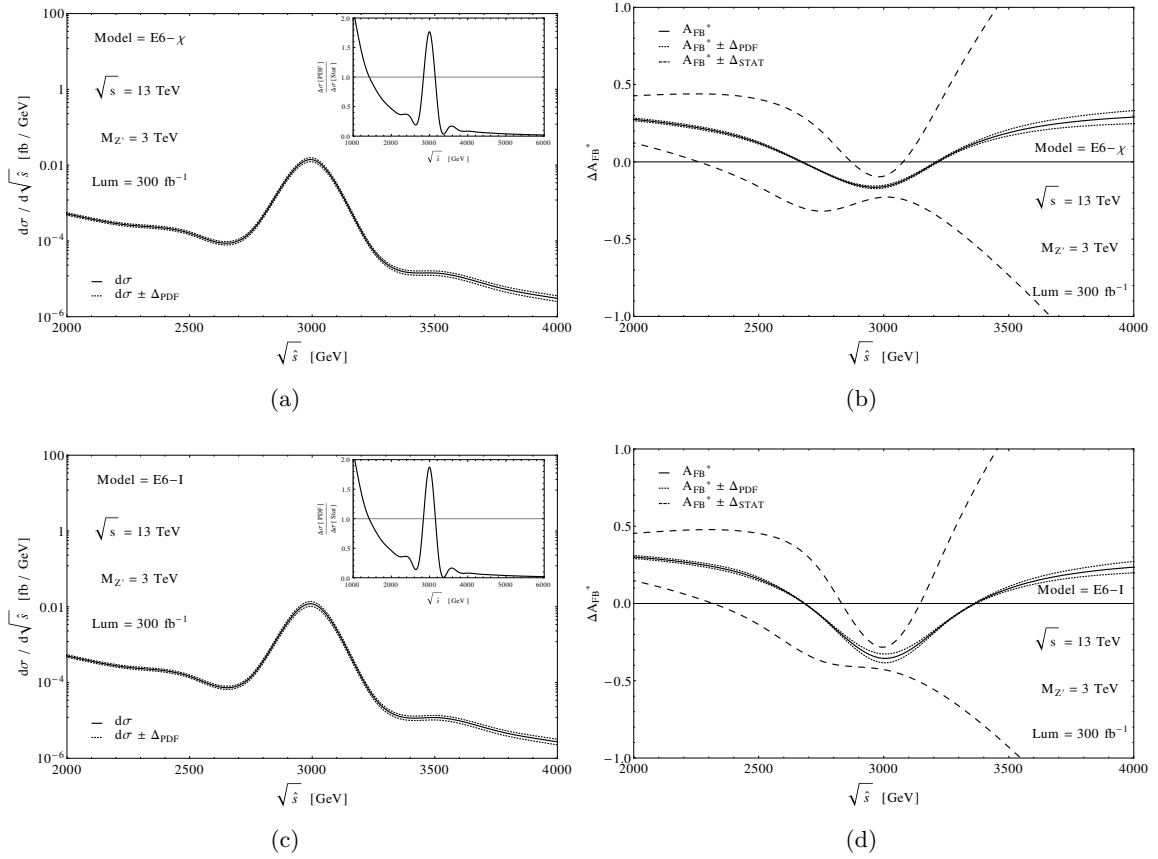
Figure 16. (a) Differential cross section as a function of the di-lepton invariant mass as predicted by the E_χ model for a Z'-boson with mass $M_{Z'} = 3\,\mathrm{TeV}$. The results are for the LHC at $\sqrt{s} = 13\,\mathrm{TeV}$ and $\mathcal{L} = 300\,fb^{-1}$. The solid line shows the central value, the dotted line the PDF uncertainty. The inset plot displays the ratio between PDF and statistical errors. (b) A_{FB}^* as a function of the di-lepton invariant mass as predicted by the E_χ model for a Z'-boson with mass $M_{Z'} = 3\,\mathrm{TeV}$. The results are for the LHC at $\sqrt{s} = 13\,\mathrm{TeV}$ and $\mathcal{L} = 300\,fb^{-1}$. The dotted lines show the PDF error band, while the dashed lines define the statistical error band. (c) Same as (a) for the E_I model. (d) Same as (b) for the E_I model.

To be more quantitative, we take figures 11(a) and 11(c). There, owing to the decreased statistical error when compared to figures 12(a) and 12(c), we have an a priori statistical significance $S \simeq 12$ around the peak of the binned cross section which would allow to claim for a new physics discovery. However, the total theoretical error does not improve much with $\mathcal{L}$, being dominated by PDF's uncertainties. Indeed, in this case, the PDF error would be two times the statistical one (see figure 16). The capability of interpreting the results of an experiment is thus significantly reduced by PDF's uncertainties in the bump search. This result should be compared with the outcome from an A_{FB}^* measurement, which is shown in figures 11(b) and 11(d). Here, owing to the higher luminosity, the experimental significance is about $S \simeq 7$ (including only the statistical error). Such an increase with $\mathcal{L}$ would be moreover followed by a proportional reduction of the theoretical error that in this case is purely dominated by statistics. Up to a large extent, the AFB is therefore a PDF
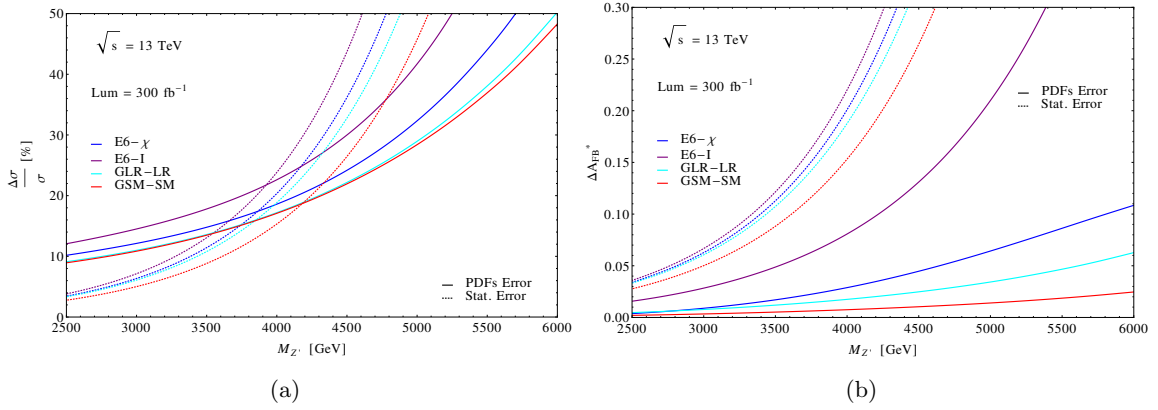
Figure 17. (a) Cross section integrated around the Z'-boson mass ($|M_{l\bar{l}} - M_{Z'}| \leq 0.05 \times E_{\text{LHC}}$) as a function of $M_{Z'}$ as predicted by the E_χ, E_I, GLR–LR and GSM–SM models. The results are for the LHC at $\sqrt{s} = 13$ TeV and $\mathcal{L} = 300\,fb^{-1}$. Solid lines represent the PDF uncertainty, dashed ones the statistical error. (b) A_{FB}^* integrated around the Z'-boson mass ($|M_{l\bar{l}} - M_{Z'}| \leq 0.05 \times E_{\text{LHC}}$) as a function of $M_{Z'}$ as predicted by the E_χ, E_I, GLR–LR and GSM–SM models. The results are for the LHC at $\sqrt{s} = 13$ TeV and $\mathcal{L} = 300\,fb^{-1}$. Solid lines represent the PDF uncertainty, dashed ones the statistical error.

safe observable. For these reasons, even if the large-x PDF's uncertainties are considerably improved in the future, it is likely that an A_{FB}^* measurement will prove to be useful evidence in any claims of Z' discoveries using the LHC data.

Of course, one needs to consider the energy scale dependence of the PDF errors, if no refitting procedure is employed. In figure 17(a), we plot PDF and statistical errors on the total cross section integrated around the mass of the Z'-boson. We integrate in the window $\pm 5\%$ E_{LHC} around the hypothetical $M_{Z'}$ where interference and finite width effects can be neglected. In evaluating the statistical error, we assume the design value for the luminosity: $\mathcal{L} = 300\,fb^{-1}$. We then vary the value of $M_{Z'}$ to see how statistical and PDF errors change in magnitude. We consider four theoretical frameworks: E_χ, E_I, GLR–LR and SSM. The figure shows that, up to roughly a 4 TeV scale, the cross section is dominated by the PDF uncertainty. In contrast, the asymmetry integrated in the same peak region is heavily dominated by the statistics for all possible Z' masses, as shown in figure 17(b). The strong dependence of PDF's central values and errors on the di-lepton invariant mass or energy scale also suggests that using as observable the ratio between the Z'-boson cross section and the on-peak SM Z-boson cross section R_σ, might not be entirely PDF safe. The two cross sections are indeed a few TeV a part. As a consequence, the quantity $\cos\phi$, measuring the correlation between the two variables, is not anymore equal to one as in the AFB case. Therefore, a cancellation analogous to that one in eq. (6.5) could not happen easily. This is another argument in favor of exploring the AFB as a search variable.

7 Conclusions

In this paper we have considered the scope of using AFB, the forward-backward asymmetry, in Z'-boson searches at the LHC in the di-lepton channel, i.e., via Drell-Yan production and decay. Such a variable has traditionally been used for diagnostic purposes in presence

of a potential signal previously established through a standard resonance search via the cross section. In this respect, we have shown that not imposing the commonly used cut on the di-lepton rapidity ($|Y_{l\bar{l}}| > 0$) would improve the discrimination between different Z' models. In addition, based on the observation that it is affected by systematics less than cross sections (being a ratio of the latter), we have studied the possibility of using AFB for such a purpose for a variety of Z' models, E_6, GLR, GSM, embedding either a narrow or wide resonance. The focus was on determining whether such a resonance could be sufficiently wide and/or weakly coupled such that a normal resonance search may not fully identify it and, further, whether the AFB could then provide a signal of comparable or higher significance to complement or even surpass the scope of more traditional analyses.

In both high ($\mathcal{L} = 300\,\text{fb}^{-1}$) and low ($\mathcal{L} = 30\,\text{fb}^{-1}$) integrated luminosity scenarios, we have found promising results. In the case of narrow width Z'-bosons, we have proven that the statistical significance of the AFB search can be comparable with the usual bump search. This makes it a useful observable in Z' searches. In case of an early discovery at low luminosity, an A_{FB}^* measurement could indeed valuably support an evidence in the bump search which by itself could otherwise be not robust enough. At the design high luminosities of the LHC Run II, the statistical significance of an observed bump type of structure can be large. However, the knowledge of the predicted (differential) cross section in any particular Z' model is subject to the large-x PDF errors. The current knowledge of PDFs is such that this results in large uncertainties. The A_{FB}^* on the other hand benefits from the partial cancellation of the PDF's uncertainties on cross sections, being a ratio of the latter, making it much more insensitive to PDF's errors. This increases the importance of A_{FB}^* measurements in the interpretation of any observations.

In the case of wide Z'-boson, the AFB search could have a better sensitivity than the cross section studies thanks to a more peculiar line-shape and lower systematic and PDF uncertainties. In essence, here, AFB in specific regions of the invariant mass of the reconstructed Z'-boson could be sensitive to broad resonances much more than the cross section, wherein the broad distribution of the signal seemingly merges with the background. Further, we have emphasised the fact that the AFB distribution mapped in di-lepton invariant mass can present features amenable to experimental investigation not only in the peak region but also significantly away from the latter.

We have explored the above phenomenology for all the benchmarks under study as well as assessed and used the optimised strategy for AFB reconstruction.

Acknowledgments

References

[1] E. Accomando, A. Belyaev, L. Fedeli, S.F. King and C. Shepherd-Themistocleous, *Z' physics with early LHC data*, *Phys. Rev.* **D 83** (2011) 075012 [`arXiv:1010.6058`] [ɪɴSPIRE].

[2] P. Langacker, *The Physics of Heavy Z' Gauge Bosons*, *Rev. Mod. Phys.* **81** (2009) 1199 [`arXiv:0801.1345`] [ɪɴSPIRE].

[3] J. Erler and P. Langacker, *Constraints on extended neutral gauge structures*, *Phys. Lett.* **B 456** (1999) 68 [`hep-ph/9903476`] [ɪɴSPIRE].

[4] E. Accomando, D. Becciolini, A. Belyaev, S. Moretti and C. Shepherd-Themistocleous, *Z' at the LHC: Interference and Finite Width Effects in Drell-Yan*, *JHEP* **10** (2013) 153 [`arXiv:1304.6700`] [ɪɴSPIRE].

[5] E. Accomando et al., *W' and Z' searches at the LHC*, `PoS(DIS 2013)125` [ɪɴSPIRE].

[6] A. Belyaev, R. Foadi, M.T. Frandsen, M. Jarvinen, F. Sannino and A. Pukhov, *Technicolor Walks at the LHC*, *Phys. Rev.* **D 79** (2009) 035006 [`arXiv:0809.0793`] [ɪɴSPIRE].

[7] D. Barducci, A. Belyaev, S. De Curtis, S. Moretti and G.M. Pruna, *Exploring Drell-Yan signals from the* 4*D Composite Higgs Model at the LHC*, *JHEP* **04** (2013) 152 [`arXiv:1210.2927`] [ɪɴSPIRE].

[8] Y.G. Kim and K.Y. Lee, *Direct search for heavy gauge bosons at the LHC in the nonuniversal* SU(2) *model*, *Phys. Rev.* **D 90** (2014) 117702 [`arXiv:1405.7762`] [ɪɴSPIRE].

[9] E. Malkawi and C.P. Yuan, *New physics in the third family and its effect on low-energy data*, *Phys. Rev.* **D 61** (2000) 015007 [`hep-ph/9906215`] [ɪɴSPIRE].

[10] G. Altarelli, B. Mele and M. Ruiz-Altaba, *Searching for New Heavy Vector Bosons in* $p\bar{p}$ *Colliders*, *Z. Phys.* **C 45** (1989) 109 [*Erratum ibid.* **C 47** (1990) 676] [ɪɴSPIRE].

[11] J. Erler, P. Langacker, S. Munir and E. Rojas, *Z' Bosons at Colliders: a Bayesian Viewpoint*, *JHEP* **11** (2011) 076 [`arXiv:1103.2659`] [ɪɴSPIRE].

[12] N. Arkani-Hamed, S. Dimopoulos and G.R. Dvali, *The Hierarchy problem and new dimensions at a millimeter*, *Phys. Lett.* **B 429** (1998) 263 [`hep-ph/9803315`] [ɪɴSPIRE].

[13] N. Arkani-Hamed, S. Dimopoulos and G.R. Dvali, *Phenomenology, astrophysics and cosmology of theories with submillimeter dimensions and TeV scale quantum gravity*, *Phys. Rev.* **D 59** (1999) 086004 [`hep-ph/9807344`] [ɪɴSPIRE].

[14] E. Eichten, K.D. Lane and M.E. Peskin, *New Tests for Quark and Lepton Substructure*, *Phys. Rev. Lett.* **50** (1983) 811 [ɪɴSPIRE].

[15] E. Eichten, I. Hinchliffe, K.D. Lane and C. Quigg, *Super Collider Physics*, *Rev. Mod. Phys.* **56** (1984) 579 [ɪɴSPIRE].

[16] CMS collaboration, *Search for physics beyond the standard model in dilepton mass spectra in proton-proton collisions at* $\sqrt{s} = 8$ *TeV*, *JHEP* **04** (2015) 025 [`arXiv:1412.6302`] [ɪɴSPIRE].

[17] T. Jezo, M. Klasen, D.R. Lamprea, F. Lyonnet and I. Schienbein, *NLO + NLL limits on W' and Z' gauge boson masses in general extensions of the Standard Model*, *JHEP* **12** (2014) 092 [`arXiv:1410.4692`] [ɪɴSPIRE].

[18] E. Accomando, D. Becciolini, S. De Curtis, D. Dominici, L. Fedeli and C. Shepherd-Themistocleous, *Interference effects in heavy W'-boson searches at the LHC*, *Phys. Rev.* **D 85** (2012) 115017 [`arXiv:1110.0713`] [ɪɴSPIRE].

[19] CMS collaboration, *Search for new physics in final states with a tau and missing transverse energy using pp collisions at* $\sqrt{s} = 8$ *TeV*, CMS-PAS-EXO-12-011 (2015) [INSPIRE].

[20] CMS collaboration, *Search for physics beyond the standard model in final states with a lepton and missing transverse energy in proton-proton collisions at* $\sqrt{s} = 8$ *TeV*, *Phys. Rev.* **D 91** (2015) 092005 [arXiv:1408.2745] [INSPIRE].

[21] R. Hamberg, W.L. van Neerven and T. Matsuura, *A Complete calculation of the order* α_s^2 *correction to the Drell-Yan K factor*, *Nucl. Phys.* **B 359** (1991) 343 [*Erratum ibid.* **B 644** (2002) 403] [INSPIRE].

[22] W.L. van Neerven and E.B. Zijlstra, *The* $O(\alpha_s^2)$ *corrected Drell-Yan K-factor in the DIS and MS scheme*, *Nucl. Phys.* **B 382** (1992) 11 [*Erratum ibid.* **B 680** (2004) 513] [INSPIRE].

[23] R. Hamberg, T. Matsuura and W. van Neerven, *Total cross sections for Z- and W-production*, ZWPROD program (1989–2002), http://www.lorentz.leidenuniv.nl/research/neerven/DECEASED/Welcome.html.

[24] S. Kretzer, H.L. Lai, F.I. Olness and W.K. Tung, *CTEQ6 parton distributions with heavy quark mass effects*, *Phys. Rev.* **D 69** (2004) 114005 [hep-ph/0307022] [INSPIRE].

[25] S. Godfrey and T. Martin, *Z′ Discovery Reach at Future Hadron Colliders: A Snowmass White Paper*, in *Community Summer Study 2013: Snowmass on the Mississippi. (CSS2013)*, Minneapolis, MN, U.S.A., July 29–August 6 2013 [arXiv:1309.1688] [INSPIRE].

[26] M. Carena, A. Daleo, B.A. Dobrescu and T.M.P. Tait, *Z′ gauge bosons at the Tevatron*, *Phys. Rev.* **D 70** (2004) 093009 [hep-ph/0408098] [INSPIRE].

[27] F. Petriello and S. Quackenbush, *Measuring Z′ couplings at the CERN LHC*, *Phys. Rev.* **D 77** (2008) 115004 [arXiv:0801.4389] [INSPIRE].

[28] M. Cvetič and S. Godfrey, *Discovery and identification of extra gauge bosons*, hep-ph/9504216 [INSPIRE].

[29] P. Langacker, R.W. Robinett and J.L. Rosner, *New Heavy Gauge Bosons in pp and p$\bar{p}$ Collisions*, *Phys. Rev.* **D 30** (1984) 1470 [INSPIRE].

[30] T.G. Rizzo, *Indirect Searches for Z′-like Resonances at the LHC*, *JHEP* **08** (2009) 082 [arXiv:0904.2534] [INSPIRE].

[31] M. Dittmar, *Neutral current interference in the TeV region: The Experimental sensitivity at the LHC*, *Phys. Rev.* **D 55** (1997) 161 [hep-ex/9606002] [INSPIRE].

[32] S. Alekhin et al., *The PDF4LHC Working Group Interim Report*, arXiv:1101.0536 [INSPIRE].